AD NUMBER

ADB024631

LIMITATION CHANGES

TO:

Approved for public release; distribution is unlimited.

FROM:

Distribution authorized to U.S. Gov't. agencies only; Test and Evaluation; NOV 1977. Other requests shall be referred to Air Force Weapons Lab., Attn: ALC, Kirtland AFB, NM 87117.

AUTHORITY

AFWL ltr, 7 Nov 1986

AD B024631

AUTHORITY:
AFWL etc.,
7 NOV 86

AFWL-TR-77-98

AFWL-TR-
77-98

(2)

EXPERIMENTS ON THE WAKES OF MULTIPLE NOZZLE CUSPS

Ford Aerospace & Communications Corp
Aeronutronic Division
Newport Beach, CA 92663

November 1977

Final Report

AIR FORCE WEAPONS LABORATORY
Air Force Systems Command
Kirtland Air Force Base, NM 87117

AFWL-TR-77-98

This final report was prepared by the Ford Aerospace and Communications Corporation, Aeronutronic Division, Newport Beach, California, under Contract F44620-75-C-0016, Job Order 2307Y101 with the Air Force Weapons Laboratory, Kirtland Air Force Base, New Mexico. Dr Paul J Ortwerth (ALC) was the Laboratory Project Officer-in-Charge.

When US Government drawings, specifications, or other data are used for any purpose other than a definitely related Government procurement operation, the Government thereby incurs no responsibility nor any obligation whatsoever, and the fact that the Government may have formulated, furnished, or in any way supplied the said drawings, specifications, or other data is not to be regarded by implication or otherwise as in any manner licensing the holder or any other person or corporation or conveying any rights or permission to manufacture, use, or sell any patented invention that may in any way be related thereto.

This technical report has been reviewed and is approved for publication.

Paul J Ortwerth

PAUL J ORTWERTH
Project Officer

FOR THE COMMANDER

Armand D Maio

ARMAND D MAIO
Lt Colonel, USAF
Chief, Advanced Laser Technology Division

Carl A Forbrich

CARL A FORBRICH, JR.
Major, USAF
Chief, Chemical Laser Branch

DO NOT RETURN THIS COPY. RETAIN OR DESTROY.

UNCLASSIFIED

SECURITY CLASSIFICATION OF THIS PAGE *(When Data Entered)*

(19) REPORT DOCUMENTATION PAGE	READ INSTRUCTIONS BEFORE COMPLETING FORM
1. REPORT NUMBER: AFWL-TR-77-98 AD-E200 984	2. GOVT ACCESSION NO. (18) AFWL-3BIE
4. TITLE *(and Subtitle)*: (6) EXPERIMENTS ON THE WAKES OF MULTIPLE NOZZLE CUSPS.	5. TYPE OF REPORT & PERIOD COVERED: Final Report. (13)
	6. PERFORMING ORG. REPORT NUMBER (9)
7. AUTHOR(s): (10) Anthony Demetriades	8. CONTRACT OR GRANT NUMBER(s): (15) F44620-75-C-0016
9. PERFORMING ORGANIZATION NAME AND ADDRESS: Ford Aerospace & Communications Corporation, Aeronutronic Division, Newport Beach, CA 92663	10. PROGRAM ELEMENT, PROJECT, TASK AREA & WORK UNIT NUMBERS: (16) 62601F 2307Y101 (17) X1
11. CONTROLLING OFFICE NAME AND ADDRESS: (11) Air Force Weapons Laboratory (ALC), Kirtland Air Force Base, NM 87117	12. REPORT DATE: November 1977
	13. NUMBER OF PAGES: 50
14. MONITORING AGENCY NAME & ADDRESS *(if different from Controlling Office)*: (12) 56p.	15. SECURITY CLASS. *(of this report)*: UNCLASSIFIED
	15a. DECLASSIFICATION/ DOWNGRADING SCHEDULE

16. DISTRIBUTION STATEMENT *(of this Report)*

Distribution limited to US Government agencies because of test and evaluation of military systems/equipment (Nov 1977). Other requests for this document must be referred to AFWL/ALC/Kirtland AFB, NM 87117

17. DISTRIBUTION STATEMENT *(of the abstract entered in Block 20, if different from Report)*

18. SUPPLEMENTARY NOTES

19. KEY WORDS *(Continue on reverse side if necessary and identify by block number)*

fluid mechanics
lasers
wakes
transition

20. ABSTRACT *(Continue on reverse side if necessary and identify by block number)*

The objective of this work is to provide basic gas-dynamical information on the wakes of nozzle cusps such as employed in gas-dynamic-laser nozzle arrays. A three-nozzle array was designed, built and installed in the Aeronutronic Supersonic Wind Tunnel. Test runs were made to check the overall performance of the nozzle-diffuser system at Mach 4, nozzle exit Reynolds number of 100,000 and nozzle wall temperatures down to 60% of stagnation, in continuous airflow. Diagnostics consisted of spark-schlieren photography, pitot and static pressure

(over)

DD FORM 1 JAN 73 1473 EDITION OF 1 NOV 65 IS OBSOLETE

UNCLASSIFIED

SECURITY CLASSIFICATION OF THIS PAGE *(When Data Entered)*

391 953

20. ABSTRACT (Cont'd)

probes, total-temperature probes and hot film anemometers. It was found that continuous unchoked flow could be obtained with a simple diffuser, and that the flow was two-dimensional even without resorting to sidewall junction tailoring. Good qualitative and fair to good quantitative agreement was found with earlier wake predictions published under the present contract. The virtual wake origin was found to lie near the nozzle throat and the near wake non-equilibrium region occupied a length equal to two nozzle exit heights beyond the trailing edge. Without cooling the wake was laminar, with long wavelength fluctuations which merit further study. With nozzle cooling transition to turbulence in the wake advanced upstream in agreement with earlier predictions of wake stability.

CONTENTS

ABBREVIATIONS AND SYMBOLS

(Note: Symbols defined below appear in the main text. Definition of symbols appearing in the Appendices can be found in the latter.)

A	:	test section cross-section area
A_D	:	cross-section area at diffuser throat
b	:	flow width
f	:	frequency
h_1	:	nozzle exit height
M	:	Mach number
p_i	:	pump inlet (diffuser exit) pressure
p_o	:	stagnation pressure
r	:	density defect
Re	:	Reynolds number
Re'	:	unit Reynolds number
Re_x	:	wetted length Reynolds number
SWT	:	supersonic wind tunnel
t	:	temperature defect
T	:	static temperature
T_o	:	stagnation temperature
Tw	:	nozzle wall temperature
T.E.	:	nozzle cusp trailing edge
u	:	velocity
w	:	velocity defect
x	:	streamwise distance (zero at trailing edge)
x_o	:	wake virtual origin
y	:	vertical coordinate
z	:	lateral coordinate
γ	:	specific heat ratio
δ	:	boundary layer thickness
Δx	:	$= x-x_o$
Θ	:	total temperature defect
ρ	:	density
$(\ )_\infty$	:	conditions external to wake
$(\ )(0)$	:	conditions on wake axis (centerplane)

FIGURES

FIGURES (continued)

SECTION I

OBJECTIVES AND SUMMARY

The main thrust of this work is to predict the wake development on theoretical grounds, and to test these predictions by experiments in the Aeronutronic Supersonic Wind Tunnel (SWT).

The theory is in reality a summary of the knowledge on linearized compressible wake behavior for both the laminar and turbulent cases. By considering a fixed family of nozzle geometries appropriate to GDL applications, it was possible to derive general formulas for a wide range of supply pressures and temperatures, exit Mach number, type of gas and nozzle wall temperature. The formulas give the fluid velocity, temperature, etc., at any point downstream of the nozzle cusp trailing edges in nondimensional form, and the graphs and tables supplied allow one to judge the effect of the wakes in an arbitrary cavity. A limitation inherent in this theory is its weakness immediately downstream of the trailing edge, both due to the nonlinearity and the non-equilibrium period of flow adjustment.

Highly resolved experimental measurements are also being performed in the SWT to verify the theory, at least at one set of conditions: Mach 4, laminar flow, exit Re of 100,000, $\gamma = 1.4$ and variable Tw (nozzle wall temperature). A representative set of multiple nozzles was installed in the SWT, capable of internal cooling to simulate low Tw/To. Data on the mean flow properties have been obtained for adiabatic conditions on the wake centerline; a smaller volume of information already exists on the fluctuating flow with and without wall cooling. These data show fair to good agreement with the theory, and they have spotlighted those areas of the theory where obvious improvements are necessary.

In addition to these results, the wind tunnel diffusion capability of the Aeronutronic setup was found adequate. Recommendations for the extension and completion of the work are indicated.

SECTION II

EXPERIMENTAL SETUP

The supersonic portion of the nozzle contours is shaped according to the coordinates of Table 1. This contour prescription begins at the throat and terminates at the leading edge. At the throat there is a slight surface slope discontinuity. The upstream end of each cusp is a 1 inch diameter cylinder section (facing upstream, see figure 1), and the blending of this portion with the throat is accomplished via a 0.047 inch radius cylinder section. Overall length of each cusp is 3 inches, width 3.10 inches and trailing edge thickness is 0.01 inches.

Details of the nozzles appear on figures 1 and 2. Two half-cusps were also built, consisting of the two symmetric halves of a regular cusp, for attachment on the floor and ceiling of the test section. When assembled, the array thus consists of three complete two-dimensional DeLaval nozzles, each of throat height 0.0945 inches, exit height 1.113 inches, width 3.10 inches and length 2.855 inches (from throat to T.E.) The arrangement is shown on figure 2 and the nozzle design method is explained in Appendix A.

The array is installed in the test section of the Aeronutronic Division Supersonic Wind Tunnel (AD/SWT), which is 3.369 inches high and 3.10 inches wide (figure 3). The approach section upstream of the nozzles is 6 inches long, and is preceded by a gradual, shallow angle contraction (about 2 feet long) bringing the air supply from the large stilling tank of the facility. In this fashion the supply air flow is parallel and free of vortices and other anomalies dangerous to the uniformity of the stream.

The rectangular cross section continues for about 12 inches downstream of the array T.E. (this is the "cavity" proper) at which point the air enters the supersonic diffuser. No effort was made to change the diffuser from its normal, fixed configuration, which consists of a two-dimensional constriction caused by floor and ceiling "ramps". However, a third ramp was later added on the sidewall to constrict the throat further and improve the unchoked flow. Further details on the diffuser type and operation appear in paragraph 4.2.

Initially optical glass sidewalls were used, stretching from a point 6 inches upstream of the nozzles to the diffuser entrance. This allowed an extensive Schlieren study of the flow which proved very useful in detecting streamlines in the approach section, evaluating the nozzle flow and resolving early problems of tunnel choking. After completion of the optical studies, lucite windows were installed, especially to avoid glass breakage occurring when the nozzles were cooled. The lucite windows were geometrically similar to the earlier glass windows, allowing the same ease of visual inspection of the flow.

The method of cooling the nozzles to reduce the ratio Tw/To and study its effect, consists of circulating liquid nitrogen (LN_2) through them. The cooling channel is a single hole running through the nozzle, coaxial with the main struts supporting the nozzles on the sidewall. Cooling was confined only on the two

TABLE 1

TABLE OF PHYSICAL COORDINATES OF CUSP NOZZLES

ξ (in.)	χ (in.)	ξ (in.)	χ (in.)
0	.5142		
.0398	.4896	.1808	.4089
.052	.482	.1916	.4034
.0575	.4784	.2029	.3978
.0618	.4759	.2153	.3918
.0646	.4741	.2272	.3862
.0674	.4726	.2398	.3803
.0699	.4711	.2530	.3744
.0734	.469	.2658	.3686
.0836	.4627	.2945	.3563
.0873	.4603	.3251	.3437
.0912	.4579	.3582	.3307
.0943	.4562	.394	.3172
.0971	.4545	.4326	.3034
.100	.4527	.4748	.2889
.1025	.4511	.5215	.2742
.1074	.449	.5715	.2592
.1125	.4463	.6274	.2433
.117	.4436	.6866	.2274
.1214	.4407	.7525	.2111
.1268	.4376	.904	.1768
.137	.432	1.0888	.141
.146	.427	1.3161	.1045
.1529	.4235	1.5902	.0704
.1616	.4189	1.9317	.0407
.1704	.4143	2.3479	.0176
		2.6157	.0076
		2.8545	.005

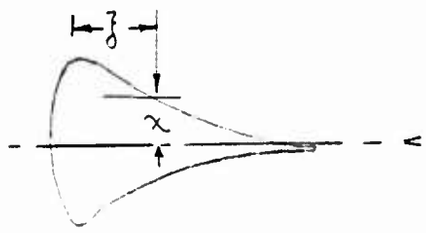

full nozzle cusps, since the half nozzles attached to the tunnel floor and ceiling could not be effectively cooled because of conduction. Two thermocouples were installed on one of the cusps to monitor its temperature, one on the forward (subsonic) portion of the cusp and the second after the nozzle throat. The coolant was drawn from LN_2 "bottles", whose capacity is adequate to produce uninterrupted wind tunnel runs lasting many hours.

SECTION III

INSTRUMENTATION

3.1 DIAGNOSTICS OF TUNNEL OPERATION AND PERFORMANCE

A group of instruments is "fixed" on the wind tunnel and monitors overall facility operation, and nozzle and diffuser operation during the run. These measure:

3.1.1 Stagnation (total or "supply") pressure Po

3.1.2 Stagnation (total or "supply") temperature To

3.1.3 Moisture content of flowing air

3.1.4 Temperatures at other points of the circuit (e.g. ambient, diffuser, etc.)

3.1.5 Pressure midway between the supersonic and subsonic diffusers

3.1.6 Pressure downstream of the subsonic diffuser

3.1.7 Barometric pressure

3.2 FLOW-FIELD INSTRUMENTATION

A minimum of three independent measurements are sufficient to define the flow field at each point. Commonly, these consist of the pitot tube, the static-pressure probe and the To probe. The pitot tubes used in this work are constrained mainly by their size (e.g. the outside diameter (O.D.) of the tip) which must meet resolution requirements, and their "hydraulic volume" which must meet time-response requirements. Adequate resolution can be obtained if the OD is less than 0.1 of the width of the shear flow in question. For almost the entire flow field in these experiments, this requirement was satisfied by the 0.02 inches OD pitot tubes used. Using thin tubing to connect the pitot tube to its transducer, the time constant could be held to 1 second or less.*

A variety of static pressure probes are available, a typical one consisting of a 0.02 inch tube tapered to a sharp point at the upstream end, with four 0.006 inches diameter holes drilled circumferencially at a distance of about 0.25 inches from the tip. Viscous interaction is computed to be negligible for this geometry.

The pitot and static pressure probes are connected pneumatically to a "pressure station" positioned outside the test section. This station mounts two absolute

*In continuous surveys (i.e. probe moving continuously) the adequacy of the response was judged by repeating the same traverse at progressively diminishing probe speeds. Maximum permissible speed was judged to be the one below which no "lag" was seen in the analog traces.

pressure transducers (0-2 psia and 0-5 psia range), a bank of Wallace-Tiernan absolute pressure gages (0-20, 0-100 and 0-400 mmHg absolute), a digital voltmeter and associated conditioning electronics, a network of valves and manifolds and a vacuum pump. These self-contained systems give great flexibility to the operator during the run. For example, the pitot or static pressure can be obtained directly as a voltage or read on the gages, or the transducer calibration can be checked quickly. Usually the transducer in use is calibrated just before and after a data-taking run. The accuracy of the Wallace-Tiernan gages is checked periodically by the Metrology Laboratory of the Aeronutronic Division. Where digital data is desired, the system output is channeled directly to the Supersonic Wind Tunnel Data Acquisition System. When connected to an analog (XY) recorder, the system can rapidly produce "pitot" maps which can reveal small details of the flow.

The total temperature is measured locally with the so-called T_o probe which is usually a bare wire thermocouple. As with all probes measuring recovery temperature, this probe is sensitive to the Mach and Reynolds number; a "recovery factor calibration" is then an important prerequisite to using this probe. This sensor also has the simplest conditioning electronics, requiring only that one thermojunction is immersed in ice.

Hot wire and film anemometers are used for the detection and measurement of turbulence. No such quantitative data were obtained in the present period, and, thus, it is unnecessary to describe the complex hardware and software needed for such quantitative measurements. Qualitative observations in these tests were made with hot film anemometers newly developed at Aeronutronic Division. Useful bandwidth for these extended to beyond 300 KHz.

SECTION IV

JOURNAL OF OPERATING CHARACTERISTICS OF THE NOZZLE ARRAY

4.1 OVERALL CHARACTER OF NOZZLE FLOW

Apart from minor corrections made in the adjustment of the nozzles, the array generally operated well from the start. Figure 4 shows a "pitot probe map" of the flow obtained at z = 0, in which the wakes and wake shocks are clearly seen. Figure 5 is the corresponding picture of the flow obtained by a one microsecond Schlieren mosaic of the flow in the cavity. In the approach section the only extraordinary feature is the apparent separation of the tunnel floor and ceiling boundary layers at the upstream ends of the half cusps. This was fully expected and does not seem to influence the flow in the upper and lower nozzles. In the nozzles themselves and beyond, one can see clearly the nozzle boundary layers and wakes, the boundary layers growing on the floor and ceiling of the cavity (test section), the wake shocks emanating at the T.E. and the diffuser inlet shocks.

4.2 TUNNEL AND DIFFUSER OPERATION

It should be mentioned at the outset that it was not the objective of this work to optimize the diffuser performance of the tunnel, but rather to operate the latter in the "unchoked" mode so that the growth of the wakes would not be disturbed.

For the type of flow pictured in figure 5, conditions were P_o = 754 mmHg and T_o = 146°F. These conditions prevailed for almost the entire set of tests done so far. However, even when these conditions were set, occasional choking of the tunnel was initially observed, pictured in figures 6 and 7. The former shows a time record of the output of the pressure transducer sensing downstream of the supersonic diffuser. When this output is of order 2 and 3 millivolts the tunnel is unchoked and choked, respectively. In this figure it is shown that the tunnel was unchoked for about 1.6 hours after start and then lapsed into a half hour period of choked flow. In the choking cycle the shocks are observed to move first to a position upstream of the supersonic diffuser inlet and progress gradually to the nozzle exits (figure 7). In the "unchoking" portion of the cycle the process reverses itself until the shock system is again expelled to a position downstream of the diffuser throat.

Since no tunnel control changes lay behind the appearance of choking, its occurrence is inexplainable. Some attempts to improve the recovery were made, consisting mainly by decreasing the diffuser throat opening from 8.3 square inches to 7.3 square inches. The latter was the opening employed throughout the tests; further efforts to improve recovery were abandoned, since several hours of continuous unchoked operation is now routinely easy to obtain in the facility.

The diffuser throat area A_D is thus 0.71 of the test section area A. The total pressure drop across the nozzle diffuser system, for P_o = 754 mmHg, is 694 mmHg,

giving p_i = 60 mmHg at the pump inlet. Thus, the operating pressure ratio is 12.5, as opposed to the normal shock ratio of 7.4 (for the design Mach 4). This corresponds to a pressure recovery of 60% of the normal shock recovery which is not bad considering that no effort was made to modify substantially the diffuser of the facility. Furthermore, the natural nonuniformity of the flow in a "GDL cavity" raises the possibility, as is now widely understood, that the recovery in diffusers with nonuniform inlet flows is not a simple problem.

4.3 NOZZLE OPERATION AND ALIGNMENT

The nozzle array operated well from the mechanical viewpoint. Some trouble was at first encountered with the method of attaching the upper and lower half-nozzles (figure 3) on the floor and ceiling of the channel. Until these were finally epoxied strongly in place, their 0.005 inch thick T.E. tended to detach from the surface and flutter with a "whistle" clearly audible to the tunnel operator.

The alignment of the nozzles was found to be critical in order to obtain an absolutely uniform flow at their exit. The procedure followed was to install the nozzles and then survey downstream of them with the pitot tube. Asymmetries found by these pitot traverses led to a readjustment of the nozzles, and the cycle was repeated until uniform flow was obtained. Criteria for "uniformity" were the symmetry of the wake profiles and of the wake shocks and their location, the identity of the growth rates of the two wakes, lateral (spanwise) uniformity, etc. In the beginning, when each sidewall was a single piece of optical glass, this iterative process was very cumbersome because probe changes also caused nozzle alignment loss (since the nozzles were disturbed when the test section probe was accessed.) Window breakage during the nozzle cooling tests prompted replacement of the glass sidewall on each side with a lucite two piece window, the upstream half of which supported the nozzles. This was the "final" nozzle support arrangement which allows once and for all fixing of the nozzles in place (during each test entry), visibility of the entire flow field* and easy access to the test section probe.

4.4 COOLING SYSTEM OPERATION

The nozzles were cooled by circulating through the liquid nitrogen (LN_2) supplied under pressure from bottles (each with 160 liter capacity.) Two thermocouples, one at the stagnation point of the cusp and another located 0.5 inches downstream of the throat and flush with the surface, indicated the nozzle temperature Tw (where Tw is usually the average of the two readings.) Low temperature would be achieved very rapidly, one minute being typically the time it took to lower the Tw to the desired value. Intermediate Tw could be obtained at will, and held steady by throttling the bottle valve. Typical operating conditions were:

*Usually, no Schlieren observations are made with this arrangement because of the poor optical properties of lucite.

Stagnation temperature To = 146°F (606°R)
Minimum Tw achieved = -100°F (360°R)
Adiabatic nozzle temperature = 90°F (550°R)
Adiabatic Tw/To = 0.91
Minimum Tw/To = 0.59

Note that the minimum Tw/To, although not excessive, is ample for the purpose of checking the Tw/To effect on wake growth which, by reference 1, is known to be important. For example, for the conditions of this experiment, (M=4, γ = 1.4) reference 1 predicts that at a distance of 10 nozzle exits the temperature defect on the wake centerline is 1.4 for the laminar adiabatic case (Tw/To = 0.9), and 1.0 for Tw/To = 0.6. Further decreases in the attainable Tw/To are thought possible by minor rework of the cooling ducts inside the nozzle cusps. (Paragraph 5.3 for the effect of Tw on transition).

During the cooling tests the flowing air dewpoint was kept, as always, at or below the -35°F mark by periodic reactivation of the tunnel's silica gel air dryer. Even so, a fine layer of frost appeared on the upstream side of the cooled cusps, but not on the nozzle surfaces. This is an indication that both friction and heat transfer is more pronounced on the latter surfaces, as assumed in reference 1. No adverse effect of this frost layer was noted on the flow.

SECTION V

EXPERIMENTAL RESULTS

5.1 NOZZLE FLOW

A profile of Mach number along $z = 0$, $x = 0$ (the nozzle exit plane) is shown on figure 8. It is seen that the design exit Mach of 4.0 has been well achieved, although on the nozzle axes ($y = 0$, $y = \pm h_1$) there is a slight increase to $M = 4.10$. A boundary layer profile at the exit is shown on figure 9, as obtained with the pitot tube. It is seen that the edge δ of the boundary layer at this position (T.E.) is almost exactly equal to 0.10 inches. A representative theoretical prediction, utilizing the formula of Low (reference 2) for laminar flow δ on a flat plate with pressure gradient,

$$\delta = 5.836 \frac{x}{\sqrt{Re_x}} \left[1 + 0.417M^2 \left(\frac{\gamma-1}{2} \right) \right]$$

gives $\delta = 0.075$ inches. This does not compare badly with the experiment, considering the theoretical approximations involved and the fact that δ as deduced from figure 9 will be larger than the actual δ due to Prandtl number effects.

This comparison indicates strongly that the nozzle boundary layers are laminar. A second indication is the shape of the pitot profile of figure 9 which is completely in character with laminar flow. A third indication, equally as strong, is that the value of the unit Reynolds number at the exit is 100,000 $inch^{-1}$, so that the wetted-length Reynolds number $Re_x = 280{,}000$. The latter is an order of magnitude below the transition Reynolds number for flat plate boundary layers, as explained in Appendix B. Using the results of this appendix, it is estimated that p_o should be increased to about 100 psia in order to achieve natural transition on the nozzle surfaces in the present experimental setup.

Figure 10 shows lateral static pressure surveys taken for the middle nozzle at its exit plane. Here the sensor was fixed first at $y = 0$ (the vertical center of the nozzle exit plane at $x = 0$) and then traversed from $z = 0.6$ inches to -0.6 inches, which includes a little less than half the span (figure 2). By thus traversing the sensor parallel to the two-dimensional nozzle throat, possible departures from flow two-dimensionality can be revealed. The absolute level of the static pressure for this p_o (=754 mmHg abs) at $M = 4$ is also clear in the figure. Following the traverse for the middle nozzle (labeled "y=0" in the middle of the figure), the traverses for the lower (at left, for $y = -0.97$") and the upper ($y = +0.97$") nozzle are shown. A small disturbance at the edge of the $y = -0.97$ inches trace is the only exception to an otherwise very smooth two-dimensional flow picture. This disturbance is due to the "throat wave" emanating from the intersection of the middle nozzle throat and the wind tunnel sidewall. It is not clear from the work done so far that such throat waves

emanate from all such intersections, but the disturbance is in anyway small, as the figure indicates.

Figure 11 shows the measured Mach number along the centerline of each of the three nozzles as far downstream as $6h_1$. There is a small systematic decrease of M, but more serious is the appearance of disturbances which cause local M variations of order 10%. At least part of this problem is suspected to be due to waves emanating from the wind tunnel sidewalls (floor and ceiling). Figure 12 shows additional measurements of Mach number in and downstream of the nozzles. The upper part of the figure shows data along the three centerlines ($y = z = 0$) and the bottom part shows profiles along y both along the vertical line $x = z = 0$ and at $2.4h_1$ downstream of the nozzle exit.

In summary, the comments made in this Section, and an inspection of the accompanying figures, reveal the following for the nozzle flow:

1. The design Mach number goal was achieved within a few percent.
2. Good two-dimensionality and repeatability is achieved.
3. Laminar boundary layers exist on the nozzles.
4. Within certain small deviations, supersonic flow is maintained in the cavity and at the nozzle exit Mach number for a distance of at least 6 times the nozzle exit heights.

5.2 QUANTITATIVE WAKE MEASUREMENTS

In the present test series, quantitative wake measurements were done within the following matrix:

$P_o = 754$ mmHg abs

$T_o = 146^oF$

$y = \pm 0.561h_1$

$z = 0$

$0 < x < 6h_1$

$Re'_\infty = 97{,}200$ inch^{-1} (nominal)

$M_\infty = 4$ (nominal)

$Tw/To = 0.92$

which indicates that the centerline ("axis" or "centerplane") of the upper and lower wakes were probed at near adiabatic (uncooled) conditions.

Figure 13 shows the measured variation of static pressure p and local total temperature To. The former generally increases away from the T.E., an indication of the expected flow "slowdown" as the diffuser entrance is approached. "Bumps" in this distribution are not bad, considering that p is an extremely sensitive parameter. For example, it has been calculated that the pressure increase shown in $1.8 < x/h_1 < 2.7$ for the lower wake would be generated by a "shock generator" of wedge angle $\sim 1.5^{\circ}$. Such small flow deflections are typical of what is expected for the present setup; e.g., at the backward facing step of the nozzle T.E. It is doubtful that any substantial improvement in the pressure distribution could be made even if more effort were to be invested into nozzle design improvement. The wake T_o variation, shown on the same figure, shows the characteristic drop below the T_{o_∞} level and the gradual increase downstream.

The important question in this work is whether the wake behavior agrees with the theoretical predictions, now collected in reference 1. This reference indicates that the velocity, temperature, density, and total temperature defects w, t, r and Θ respectively, defined by

$$w \equiv \frac{u_\infty - u(0)}{u_\infty}$$

$$t \equiv \frac{T(0) - T_\infty}{T_\infty}$$

$$r \equiv \frac{\rho_\infty - \rho(0)}{\rho_\infty}$$

$$\Theta \equiv \frac{T_o(0) - To_\infty}{T_{o_\infty}}$$

should be unique functions of the coordinate $\Delta x/h_1$, where $\Delta x \equiv x - x_o$ is the distance from the virtual wake origin x_o (and h_1 is the nozzle exit height). Thus, to compare the values of w, r, t, etc., measured in this experiment with the theoretical predictions it is important, first, to see where the origin x_o lies according to the experiment.

5.2.1 DETERMINATION OF THE VIRTUAL ORIGIN FROM THE DATA

The procedure to be followed is: (a) a test is first made to see if the relation

$$w, t \sim (x - x_o)^{\frac{1}{2}} \qquad (1)$$

holds, (b) points lying close to the T.E. and not obeying the above relation are excluded from partaking in the finding of the origin x_o, (c) a computer least-squares fit of the remainder of the points is made and x_o is found.

Figure 14 shows the w, r, t plots versus $\Delta x/h_1$. For the moment we will use this figure to test the validity of the theoretical prediction (1). Indeed, this relation is seen to be achieved if the first six points (at the lowest $\Delta x/h_1$) are excluded. Leaving figure 14 aside for a moment, make a second test of the relation (1) by plotting, more conveniently, the inverse square of w and t, for both wakes, on figure 15, versus x/h_1. Open symbols in this plot are the "excluded" six points in each case. All other points (solid symbols) were computer least-squares fitted into a straight line. The intersections of these lines with the abscissa should give the virtual origin x_o. There are differences for the upper and lower wakes as follows:

Upper wake:

Velocity-defect determination: $x_o = -3.6h_1$

Temperature-defect determination: $x_o = -3.8h_1$

Average: $-3.7h_1$

Lower wake:

Velocity-defect determination: $x_o = -0.6h_1$

Temperature-defect determination: $x_o = -1.2h_1$

Average: $-0.9h_1$

Average for both wakes: $x_o = -2.3h_1$

The large spread obtained between the two wakes is less than satisfactory, although it is clear that x_o lies upstream of the T.E. As a temporary measure, therefore, proceed by adopting the theoretically predicted value $x_o = 2.5h$ which is close to the "grand average."

5.2.2 VARIATION OF THE MEASURED DEFECTS

The data on the measured values of w, t, r and ϑ are shown on figures 14 and 16. These plots show information additional to that of figure 15 in that the r and ϑ are now included, the coordinates are logarithmic, and use has been made of the fact that the effective origin lies at $x_o = 2.5h_1$. In this way, for example, the first point taken, at $x = 0.061h_1$, is shown on figure 14 to lie at $\Delta x/h_1 = 2.5 + 0.061 = 2.561$. In this way, the curves for the theoretical predictions from reference 1 have been drawn in for comparison, since in this theory it was also assumed that $x_o = -2.5h_1$ for the conditions M_∞, γ, etc., of the present experiment. Furthermore, two sets of curves are shown for the theory (solid and dashed); the dashed curves correspond to predictions for the

design conditions $M_\infty = 4.0$, $\gamma = 1.4$, $T_w = T_o$. The solid curves show the predictions for the flow conditions actually obtained (which were slightly different from design) as follows: $M_\infty = 3.75$*, $T_w \simeq 0.9\ T_o$.

The main results from figures 14 and 16 are twofold: first, there is a clear agreement with the one-half power wake decay law, and the location and extent of the nonequilibrium region is also clear; these findings were already gleaned from figure 15. The second important result is that there is some disagreement with the theoretical predictions. Specifically, it appears that the measured defects are about 50% lower than the predictions, on the average. From this finding it is tentatively concluded that the theory is not especially accurate. An examination of the basis of the theory (reference 1) shows that the latter includes linearization and a few other subtle assumptions which are normally "safe". The present results indicate the need for improving the theory.

It should be noted that the observed disagreement is in a very sensitive type of experimental quantity, the "defect" (see the earlier definition of w, t, r and Θ). In numerical (dimensional) terms, the fluid axis velocity, temperature, etc., as measured, agrees with the predictions closely. (See discussion to this effect on p. 33 of reference 1).

An effort was made to find additional experimental data to compare with the theory of reference 1. A great number of GDL setups have already been studied, but unfortunately most studies are limited to Schlieren photography. Of those which are not, the data of Director (reference 3) provide numerical information on wake decay similar to those obtained here (Director's data concern only the density defect detected by interferometry). These results are shown on figure 17 compared with the theory; the agreement is good, and is significant because his wake was turbulent.

5.3 FLUCTUATION MEASUREMENTS WITH AND WITHOUT COOLING

Quantitative measurements of the "turbulence" of the wakes were made only in a preliminary fashion, partly because the precise measurement of turbulence is too big a task to occur so early in this research, and partly because the wake was already suspected to be laminar. A thin film anemometer was chosen, chiefly because its sturdiness makes it more suitable for exploratory work. Traverses of the rms signal were made versus y for a number of constant x and constant z.

Figure 18 shows typical results when the nozzle cusps were uncooled (e.g., $T_o = 146^\circ F$, $P_o = 754$ mmHg, $T_w = 95^\circ F$). At midspan (z=0) and a representative axial distance $x = h_1$ the figure shows the wideband sensor output, characterized of the two double peaked wake profiles. The signal between the two

*As already explained, the nozzle exit Mach number M_∞ was found a little different, 4.15 vs. 4.0, at the center of the nozzle. On the wake axis, however, the Mach number started out at about 4.0 and decreased to about 3.75 downstream. Therefore, it was felt that a good alternate estimate of the predictions would be to use $M_\infty = 3.75$.

wakes is almost exactly equal to the electronic noise, i.e., there is no sensible signal in the space bounded by the two wakes. The wake signals are higher than this noise signal by a factor of about 4. The question posed here is this: if this wake signal results from wake turbulence, then the claim of a laminar wake for these conditions is contradicted. The dilemna is resolved by studying the sensor output spectra shown on figure 18. It is seen that the energy-carrying spectrum lies below 25 KHZ. On the other hand, the "wake frequency" computed for these wakes on the basis of their width ($\sim$ 0.2" = 0.5 cm) and the edge velocity ($\sim$ 700 m/sec) is 140 KHZ, so that the spectrum should extend beyond 1 MHZ if the wake was turbulent.* Thus, the wake is indeed laminar, and the unanswered question remaining is the origin of the observed fluctuations in this laminar wake. A study of earlier experiments (reference 4) is that fluctuations in the laminar wake exist long before transition sets in.

Similar measurements were made with the nozzle cusps cooled to $T_w \simeq -80^oF$ (corresponding to $T_w/T_o \simeq 0.63$). Here it was found that the wake thickened by a factor of about 2 from x=0 to $x=6h_1$ where the fluctuation spectrum cascaded to about 300 KHZ. It, therefore, appears that the cooling action "tripped" the wake into turbulence. This confirms the well known phenomenon of wake destabilization by cooling (reference 5). Future measurements are badly needed to pinpoint the accelerated transition quantitatively.

*A practical rule for estimating the upper "active" frequency f of a turbulent shear flow is $f = 10u_e/b$, where u_e is the edge velocity and b is the flow width.

SECTION VI

INTERIM CONCLUSIONS AND RECOMMENDATIONS FOR FURTHER WORK

On the basis of the work done to date, the following conclusions can be drawn about the specific experiment performed in the AD/SWT:

(1) The wind tunnel was successfully converted into a facility for testing GDL nozzle arrays.

(2) A nozzle array was installed and tested, fulfilling its design requirements at Mach 4.0 and continuous flow.

(3) Although no design provisions were made to "tailor" the nozzle-wall intersection, good quality two-dimensional flow was achieved to $x = 6h_1$.

(4) Running time is arbitrary (e.g., several hours) with unchoked flow without drastic changes in the diffuser configuration.

(5) The cooling system can be further improved, although long duration flows at $T_w \simeq 0.6\ T_o$ can be already achieved at present.

In addition, certain general conclusions of importance to all nozzle cusp wake research can be drawn:

(6) The quantitative data taken so far are in fair-to-good agreement with a rudimentary theory of wake flows (reference 1).

(7) The virtual wake origin for nozzle cusp wakes appears to be located at the nozzle throat.

(8) Nozzle wall cooling moves turbulent transition upstream in the wake.

(9) The trailing edge nonequilibrium region occupies a length equal to about two nozzle exit heights, beyond which wake similarity is achieved.

In order of importance, the following tasks are recommended for the immediate future:

(10) Measurements of the mean (average) properties must be continued and completed. Specifically, the following must be done:

10.1 Data must be taken all the way to the diffuser entrance ($x \simeq 12h_1$).

10.2 Radial (lateral) profile data must be obtained.

10.3 A better determination of the virtual origin is possible, from the data

collected under paragraphs 10.1 and 10.2.

10.4 A complete set of data must be obtained for the cold wall case, and compared with the theory of reference 1.

(11) Turbulent wakes must be obtained and measured. Transition by artificial roughening of the nozzle surface should be possible to obtain.

(12) The cause of the observed fluctuations in the laminar wake (mentioned in paragraph 5.3) must be found by further hot wire anemometer measurements.

(13) For the turbulent wake, hot wire anemometer measurements must be combined with a set of turbulence-magnitude predictions, especially for the cold wall case, to see if it is possible to predict the fluctuations for nozzle cusp wakes (in the same fashion as the mean flow properties have been predicted by reference 1).

REFERENCES

1. Demetriades, A.: Linearized Theory of Gas-Dynamic-Laser Nozzle Wakes and Applications, Aeronutronic Ford Publication No. U-6276, Aeronutronic Ford Corp., Newport Beach, California, October 1976

2. Low, G.M. : Simplified Method For Calculation of Compressible Laminar Boundary Layer with Arbitrary Free Stream Pressure Gradient, NACA TN 2531, Washington, D.C., October 1951

3. Director, M.N.: Aerodynamic Parameters Affecting Practical Gas Dynamic Laser Design, AIAA Paper 73-626, Palm Springs, California, July 1973

4. Demetriades, A.: Observations on the Transition Process of Two-Dimensional Supersonic Wakes, AIAA J. Vol. 9, No. 11, p. 2128, November 1971

5. Demetriades, A.: Heat Transfer Effects on Supersonic Wake Transition, Physics of Fluids, Vol. 13, No. 1, January 1970

6. Shames, H., and Seashore, F.L.: Design Data for Graphical Construction of Two-Dimensional Sharp Edge Throat Supersonic Nozzles, NACA RM E8J12, Washington, D.C., December 1948

7. Coles, D.: Measurements of Turbulent Friction on a Smooth Flat Plate in Supersonic Flow, J.A.S. Vol. 21, No. 7, p. 433, July 1954

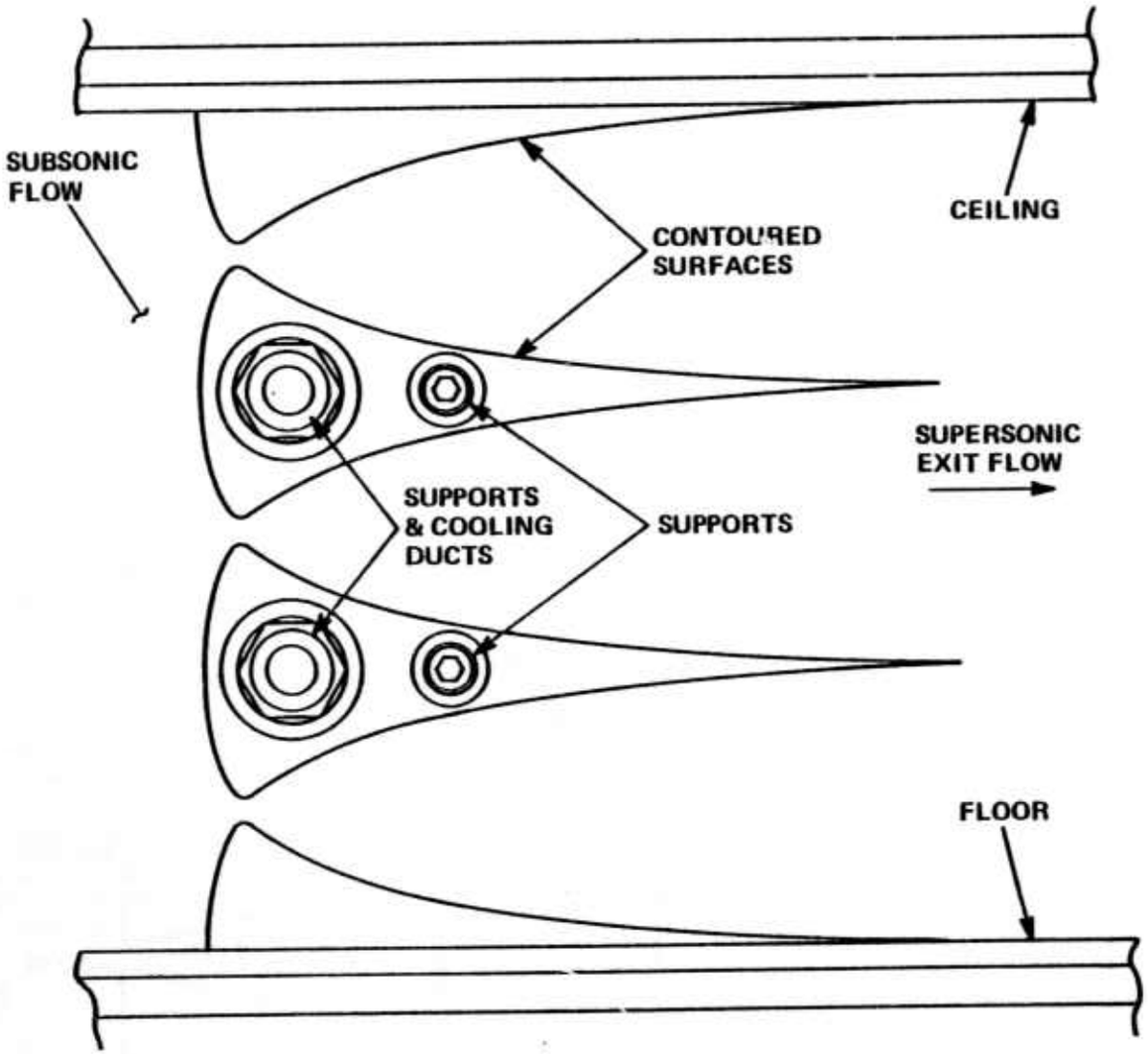

Figure 1. Drawing of nozzle-array configuration (to scale.) Flow from left to right.

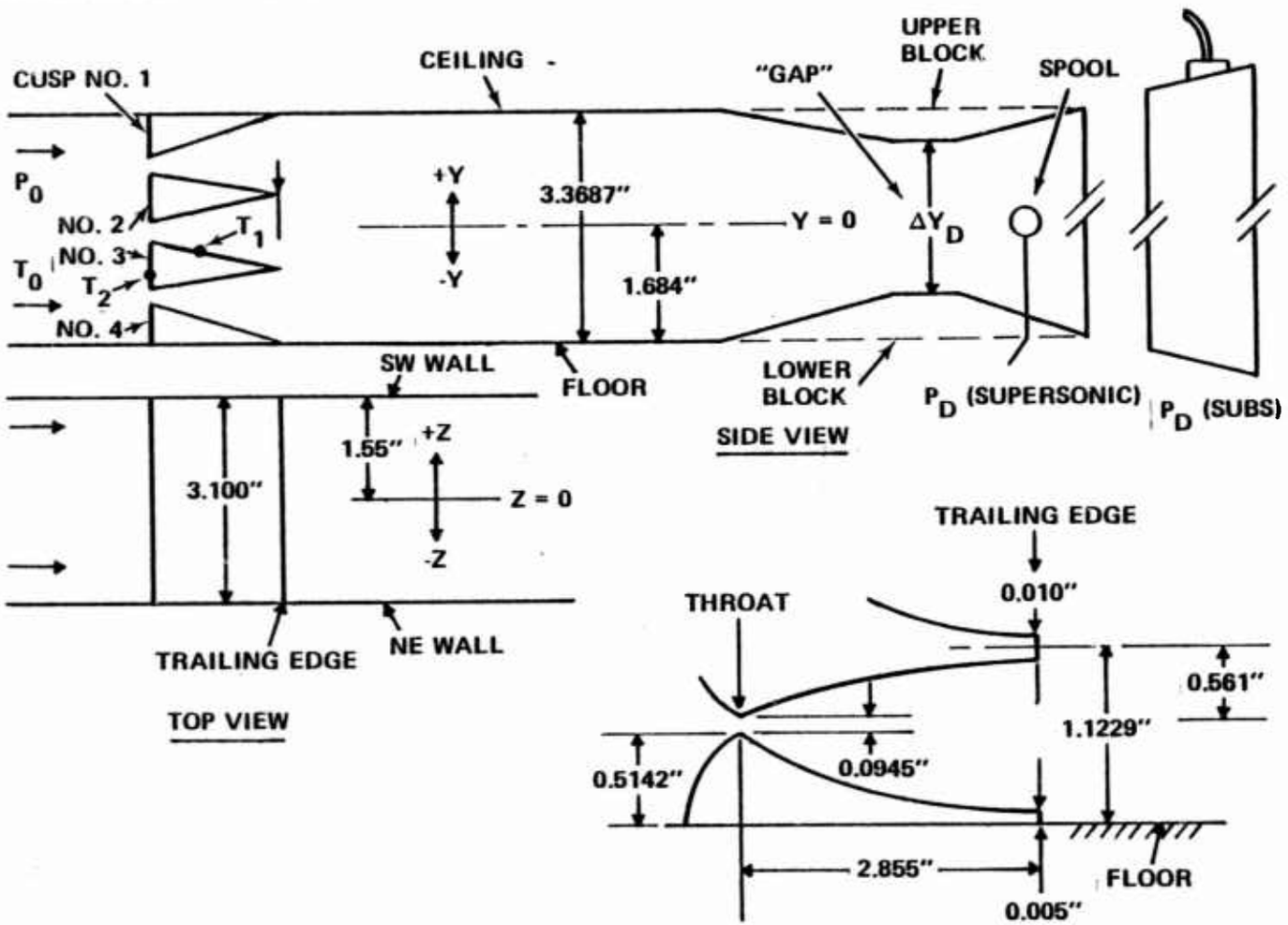

Figure 2. Schematic of test setup (not to scale) showing nozzles and diffuser with relevant dimensions and nomenclature; nozzle details at lower right.

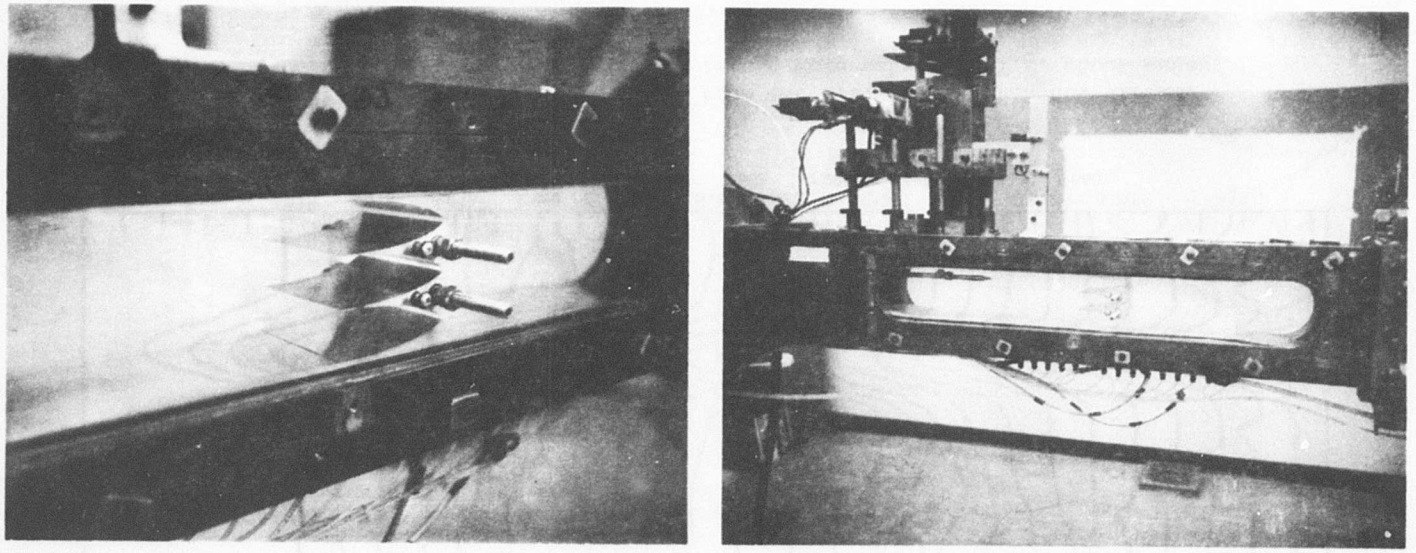

Figure 3. Left: Nozzle array as installed, looking obliquely upstream
Right: Overall view of array installation in the SWT, also showing probe and actuators at top left. Flow is from right to left,

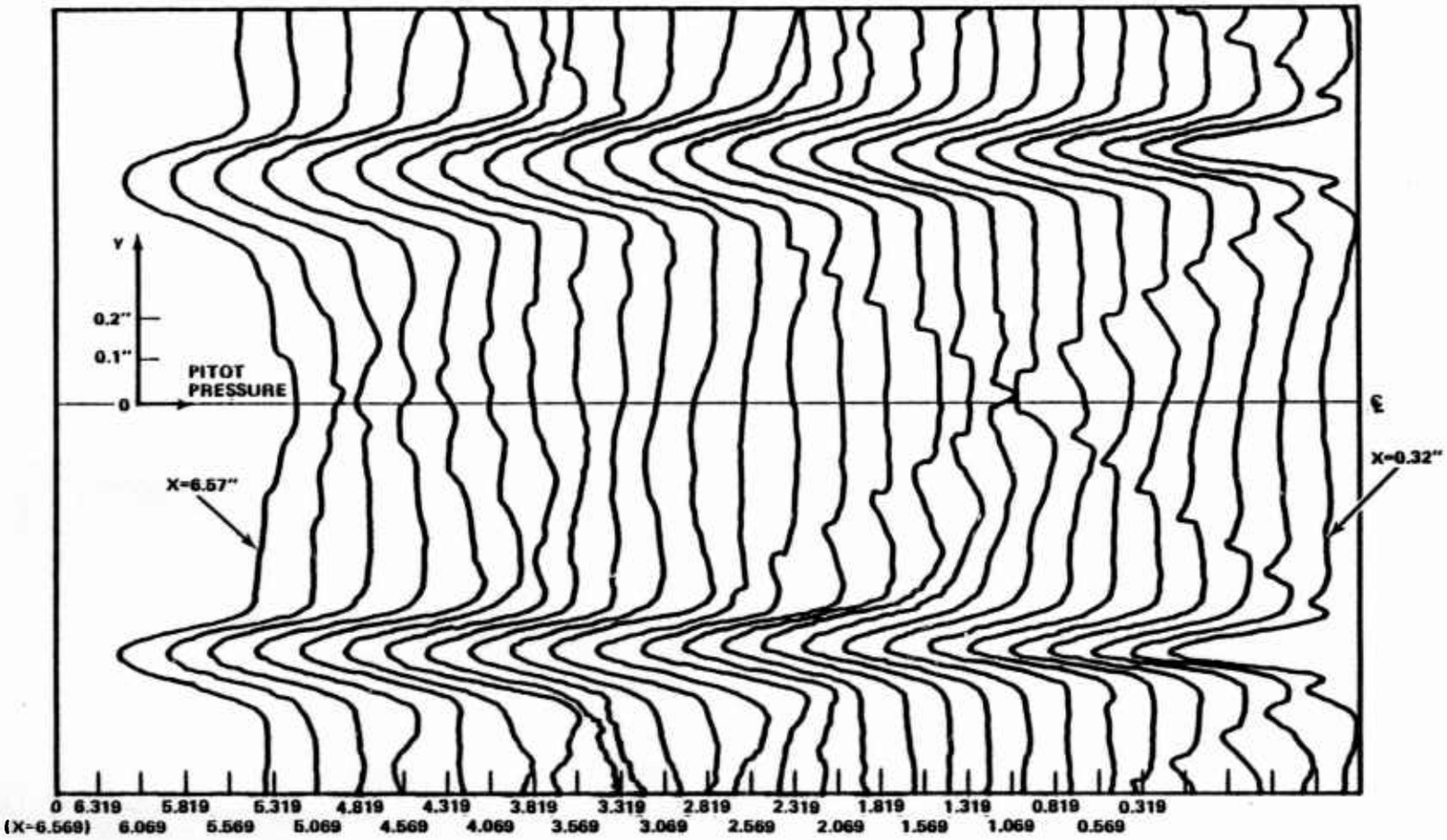

Figure 4. Pitot map of the flow from the T.E. to 6 inches downstream. Flow is from right to left. Note wakes and T.E. shock waves.

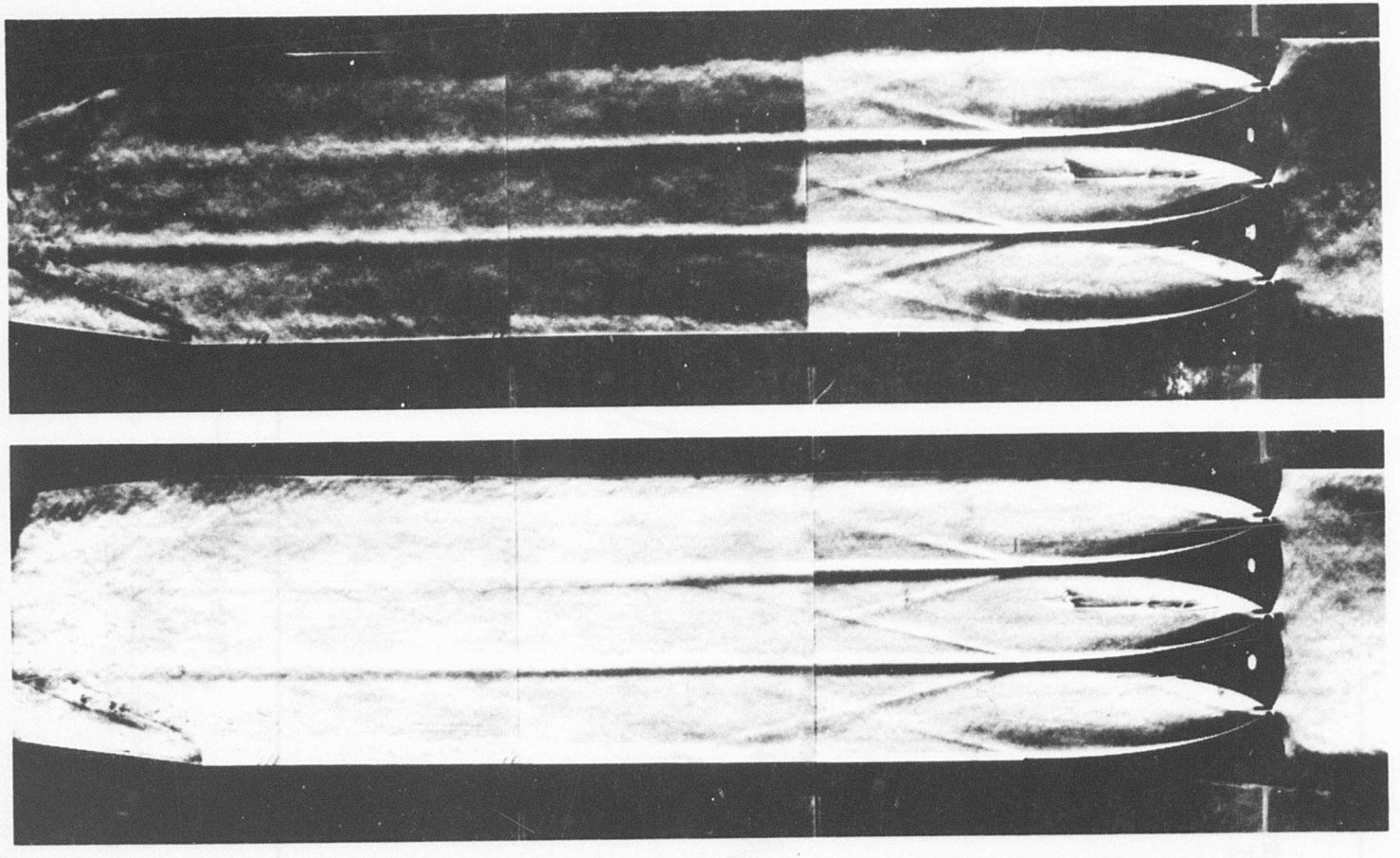

Figure 5. Spark-Schlieren photos (shown at two different contrast levels) of the flow. Note boundary layer separation in the supply chamber (at right) and diffuser inlet shocks at left.

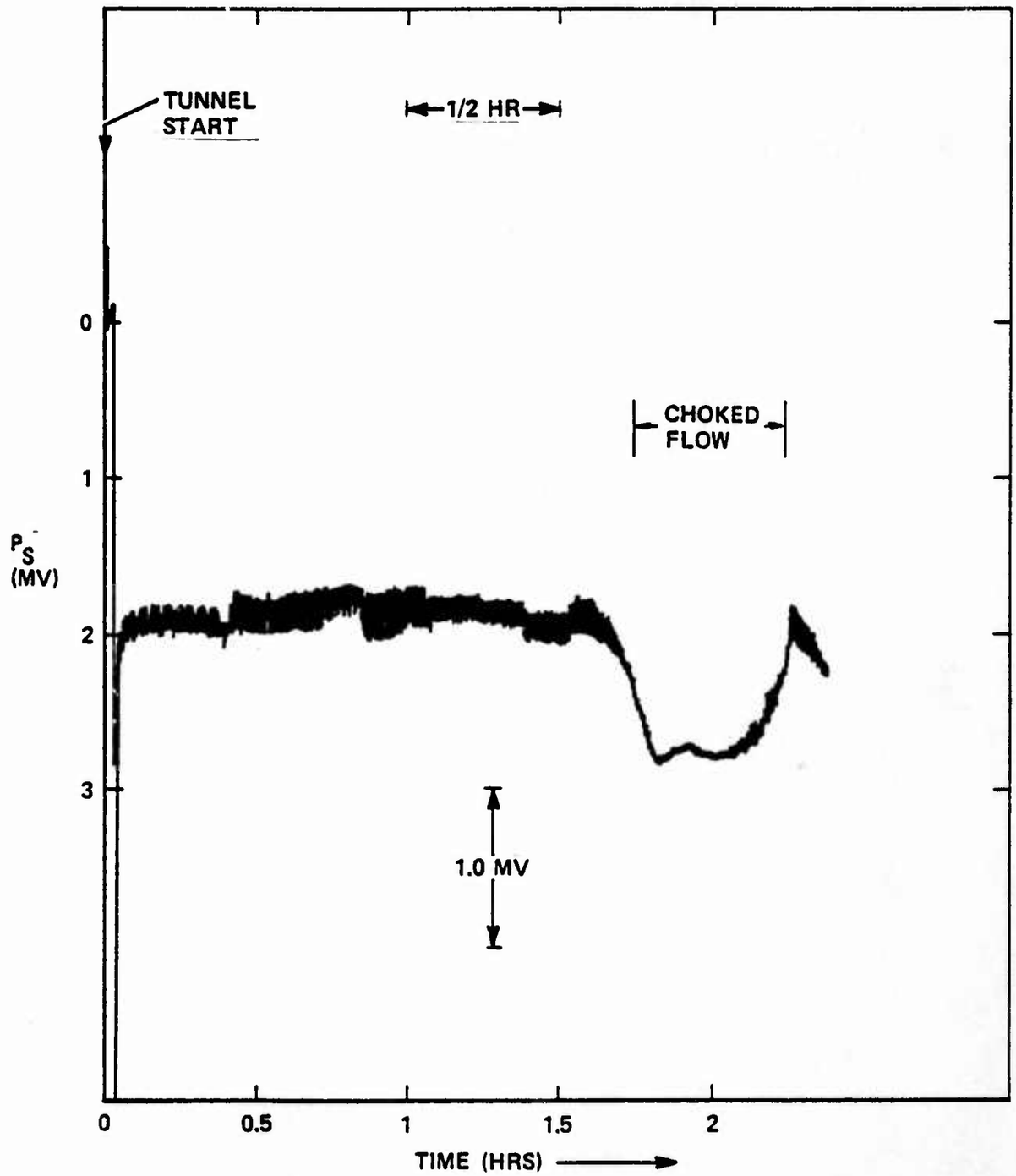

Figure 6. Time record of diffuser pressure on a typical run; flow is unchoked as long as $p_s \simeq 2$ mv.

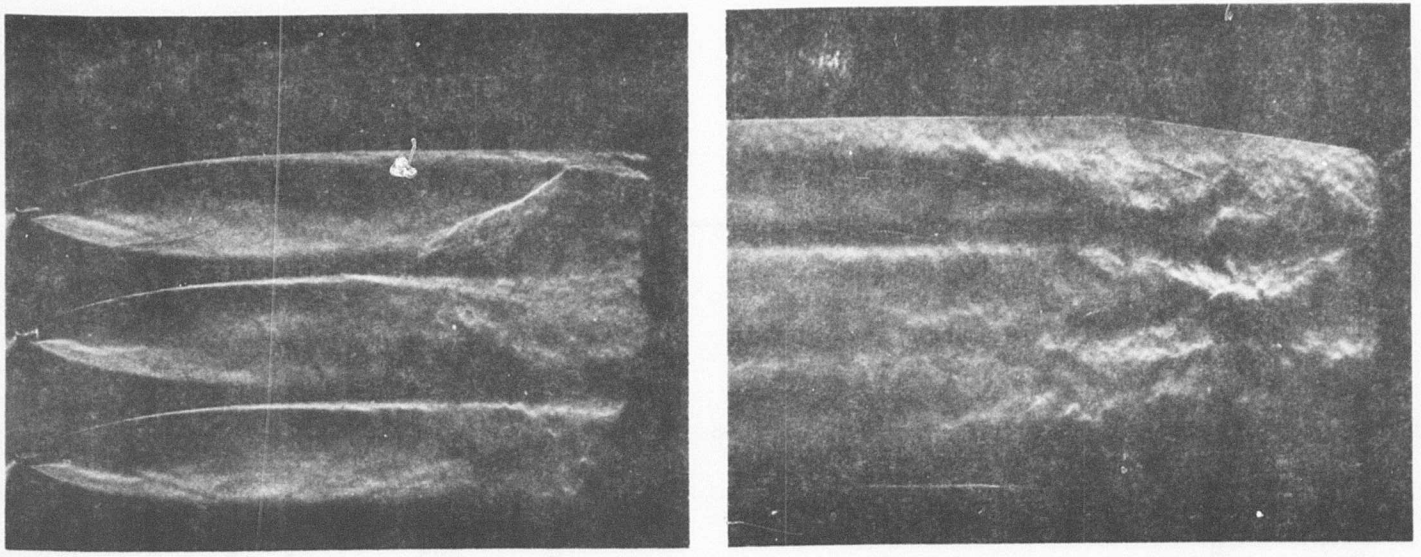

Figure 7. Typical Spark-Schlieren photos taken in the choked mode. Photo at left shows "intense" choking with shocks near the T.E. Later, shocks recede to the diffuser inlet (right) where they are shown here just before being "swallowed" and unchoking the flow.

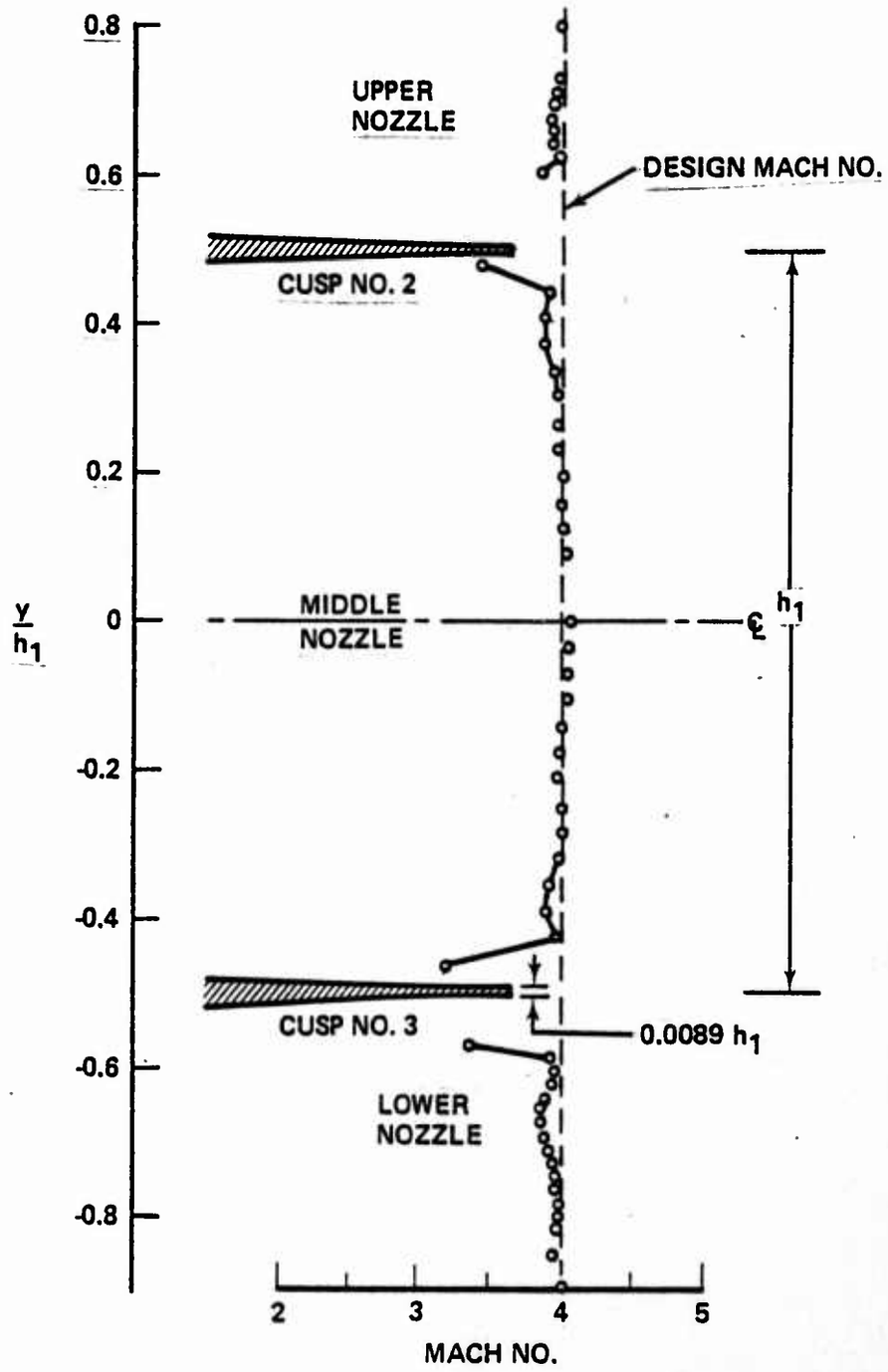

Figure 8. Measured Mach numbers at nozzle exit plane.

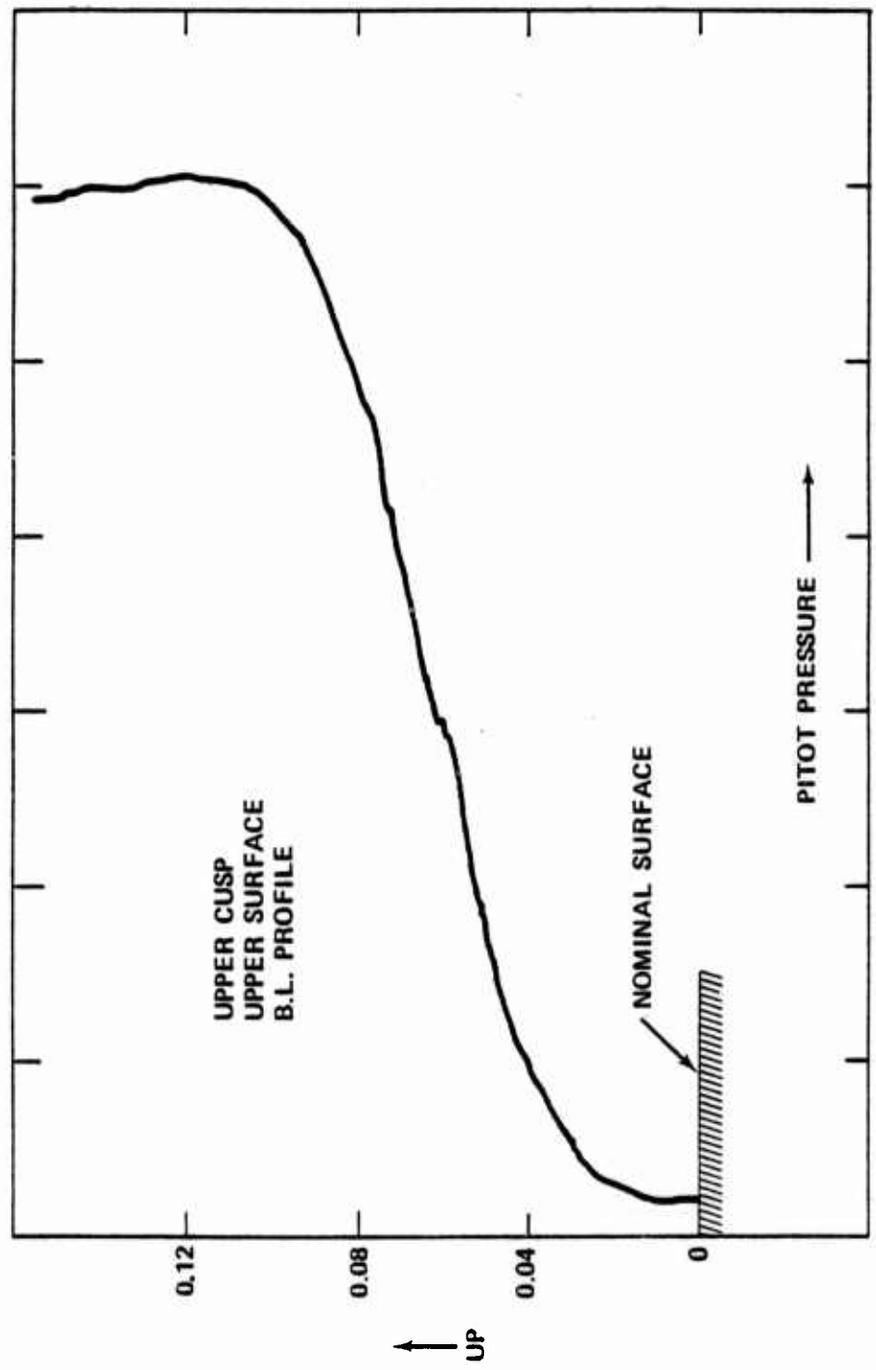

Figure 9. Typical laminar boundary layer profile measured with the pitot tube at the T.E.

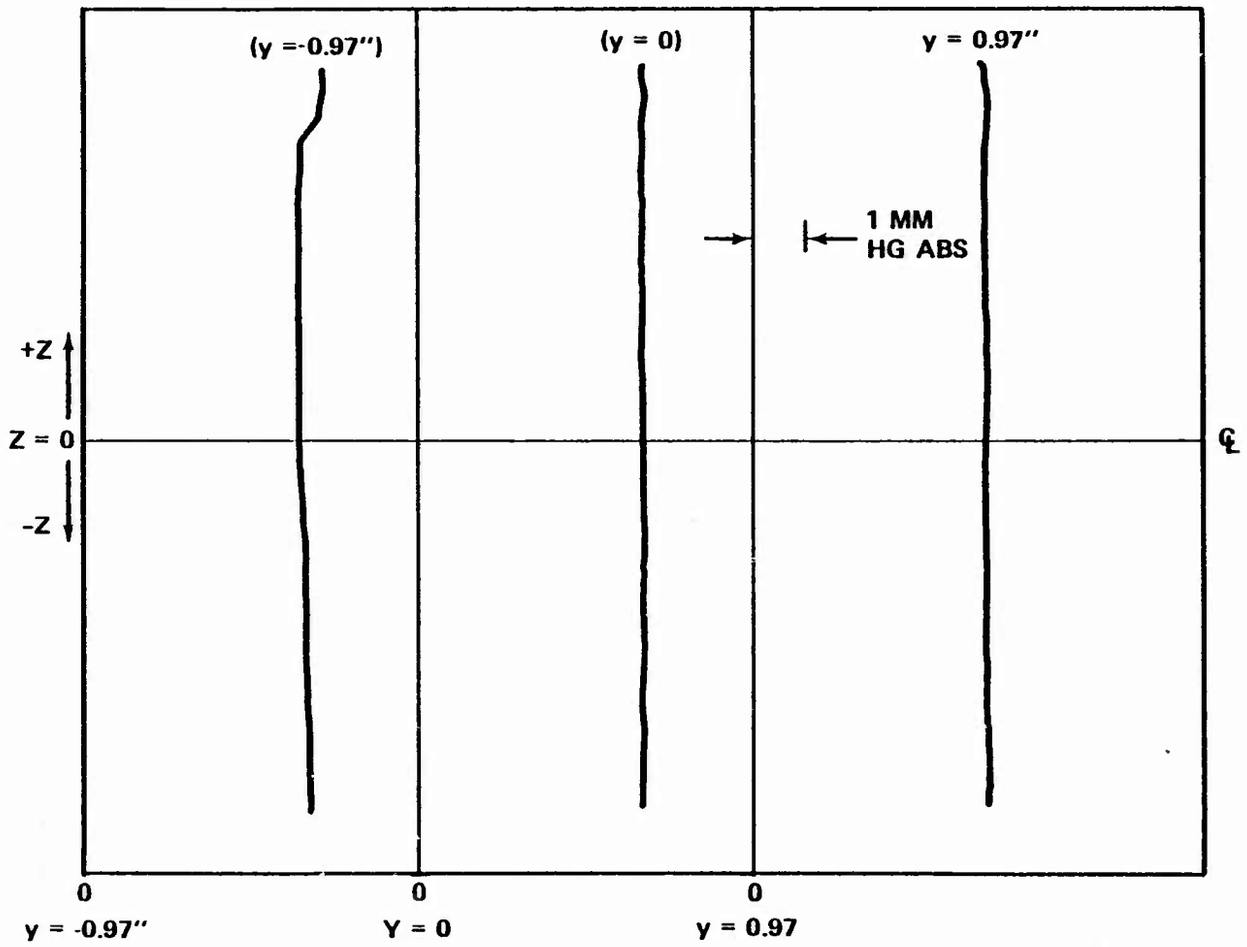

Figure 10. Typical lateral (along z) static pressure profiles at the T.E. (x = o).

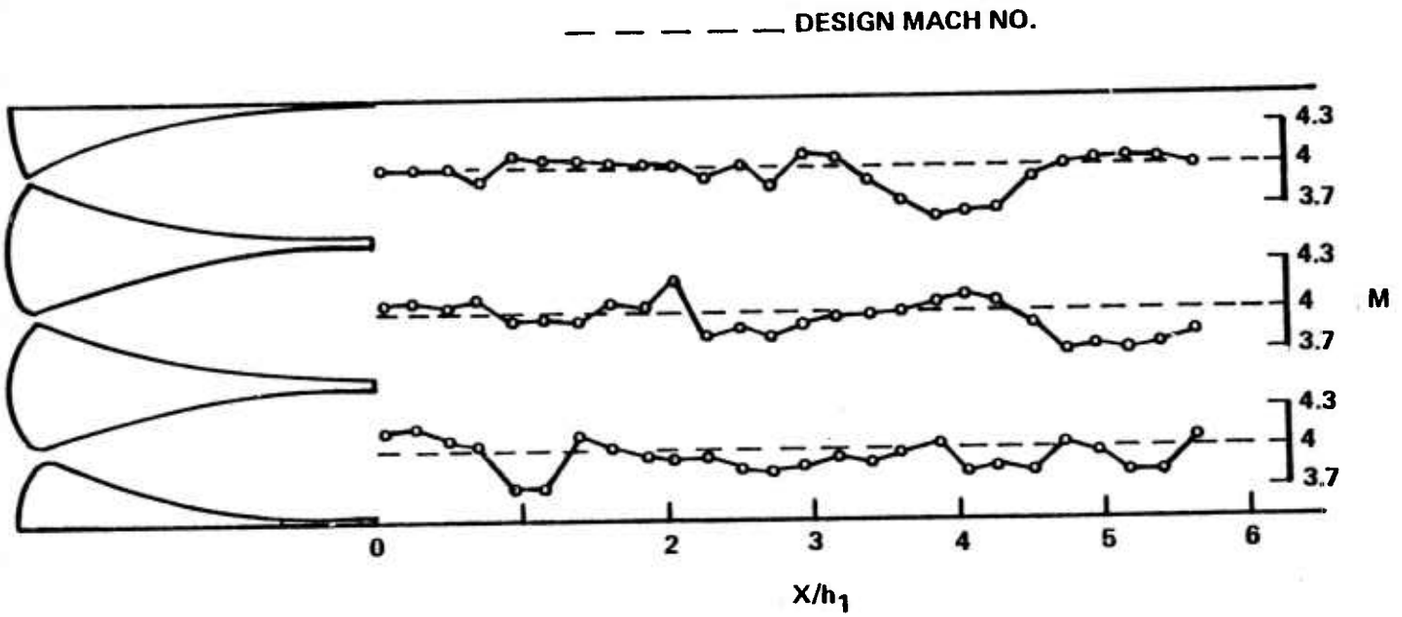

Figure 11. Mach number profiles along the three nozzle centerlines (z = o).

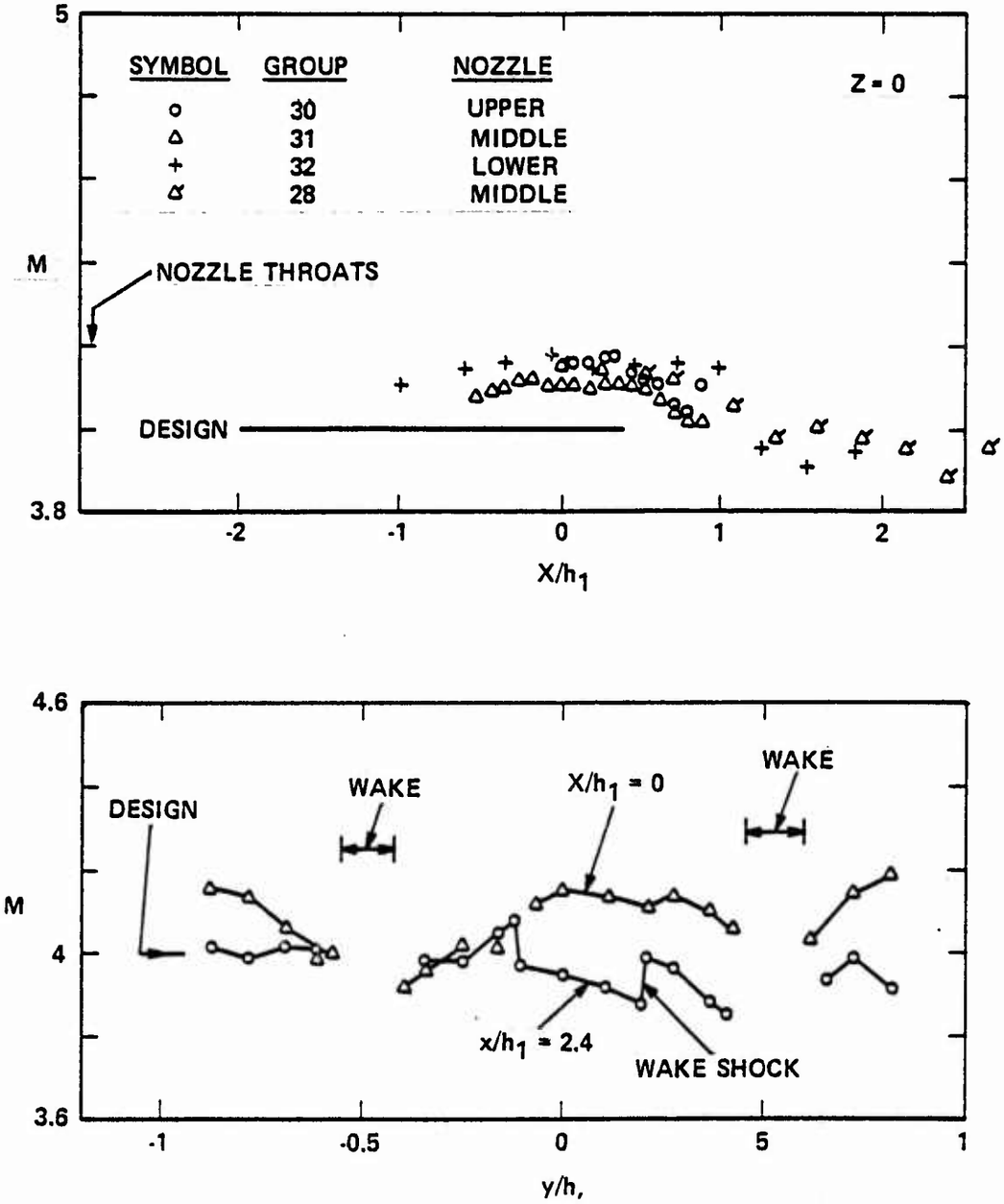

Figure 12. Top: Mach numbers measured near the T.E. of each nozzle, on the nozzle axes. Bottom: Mach number profiles at and some distance from the T.E.

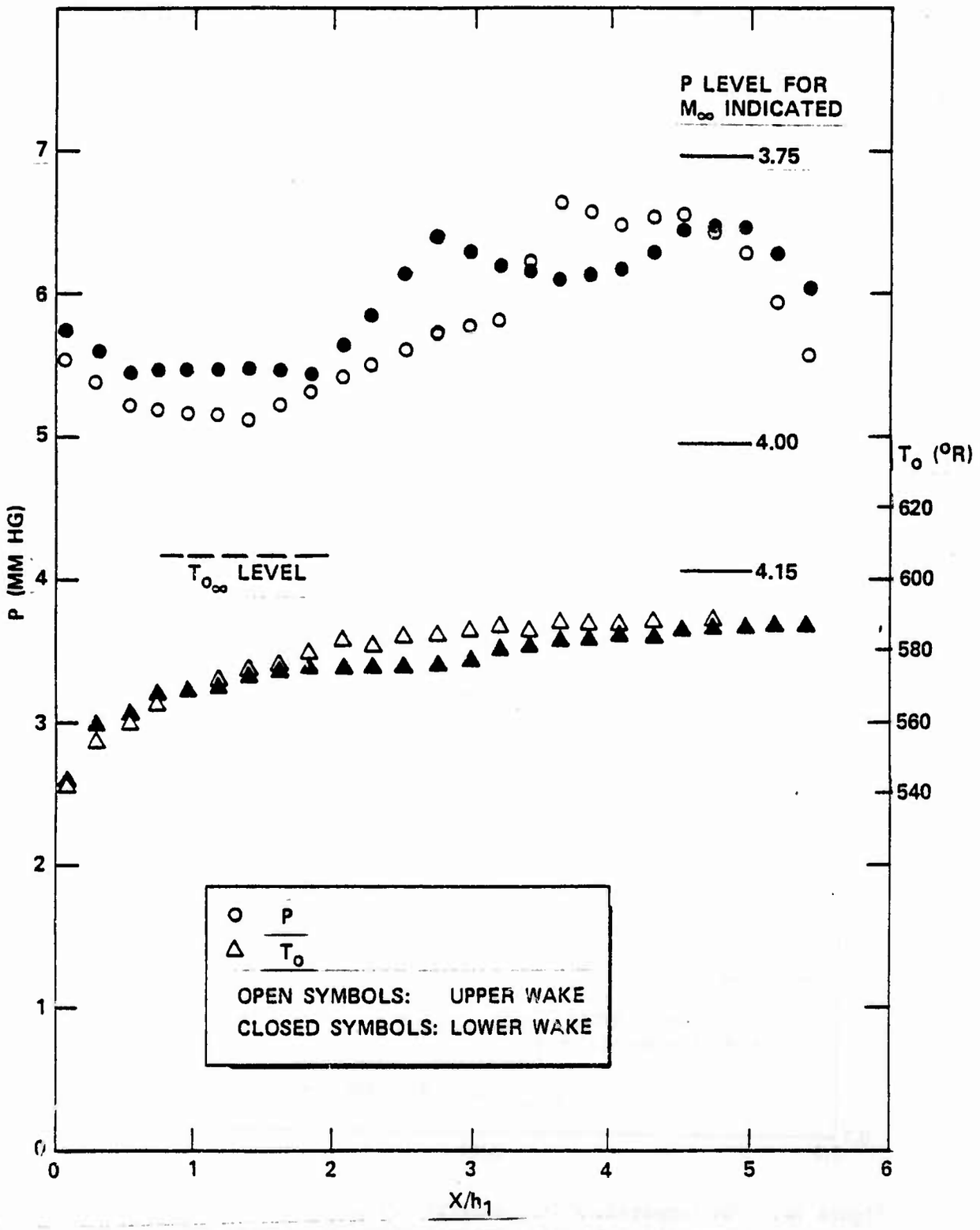

Figure 13. Static pressure and total temperature as measured along the axes of the two wakes (z - o).

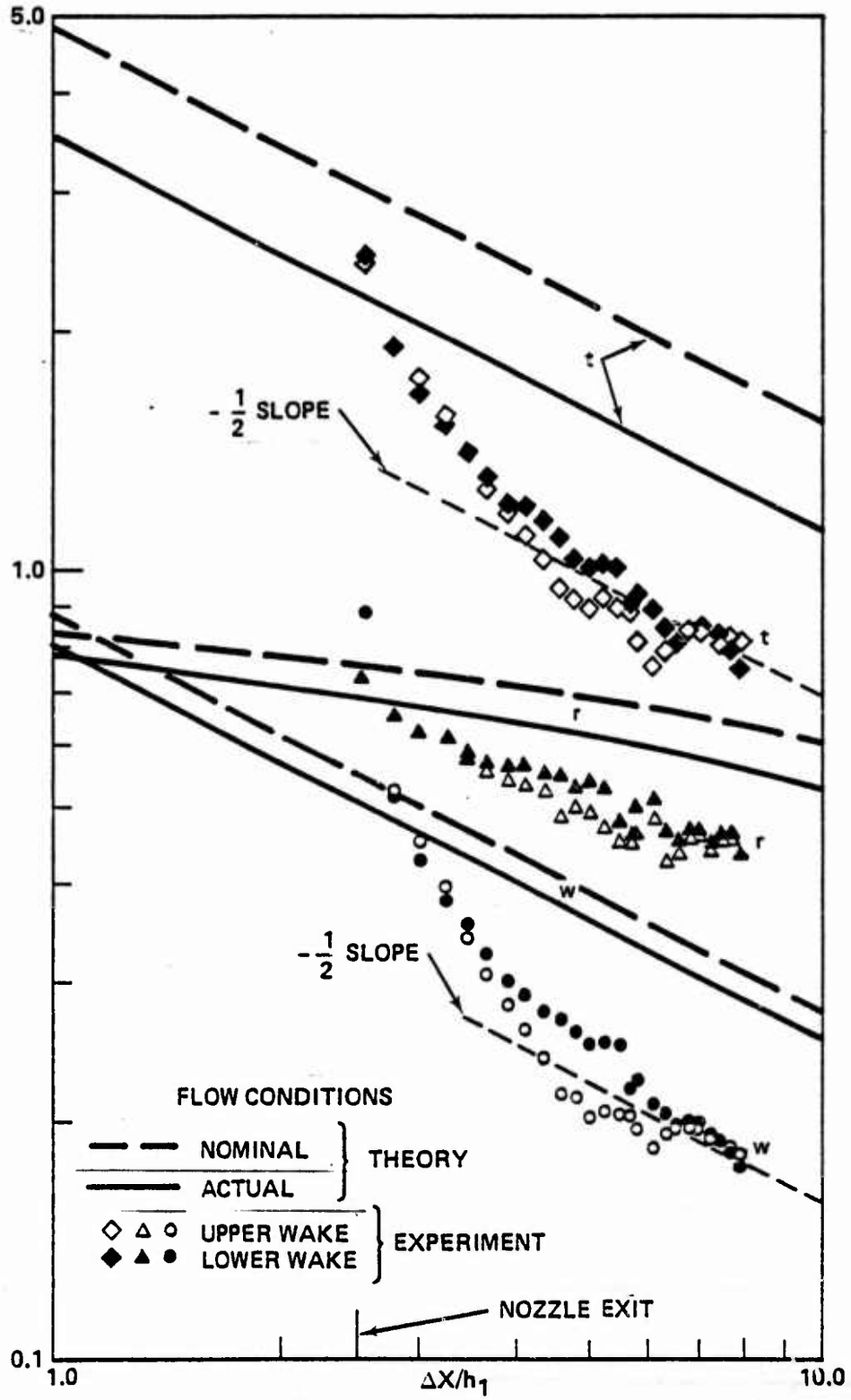

Figure 14. The temperature (t), density (r) and velocity (w) defects along the two wakes compared with theoretical predictions.

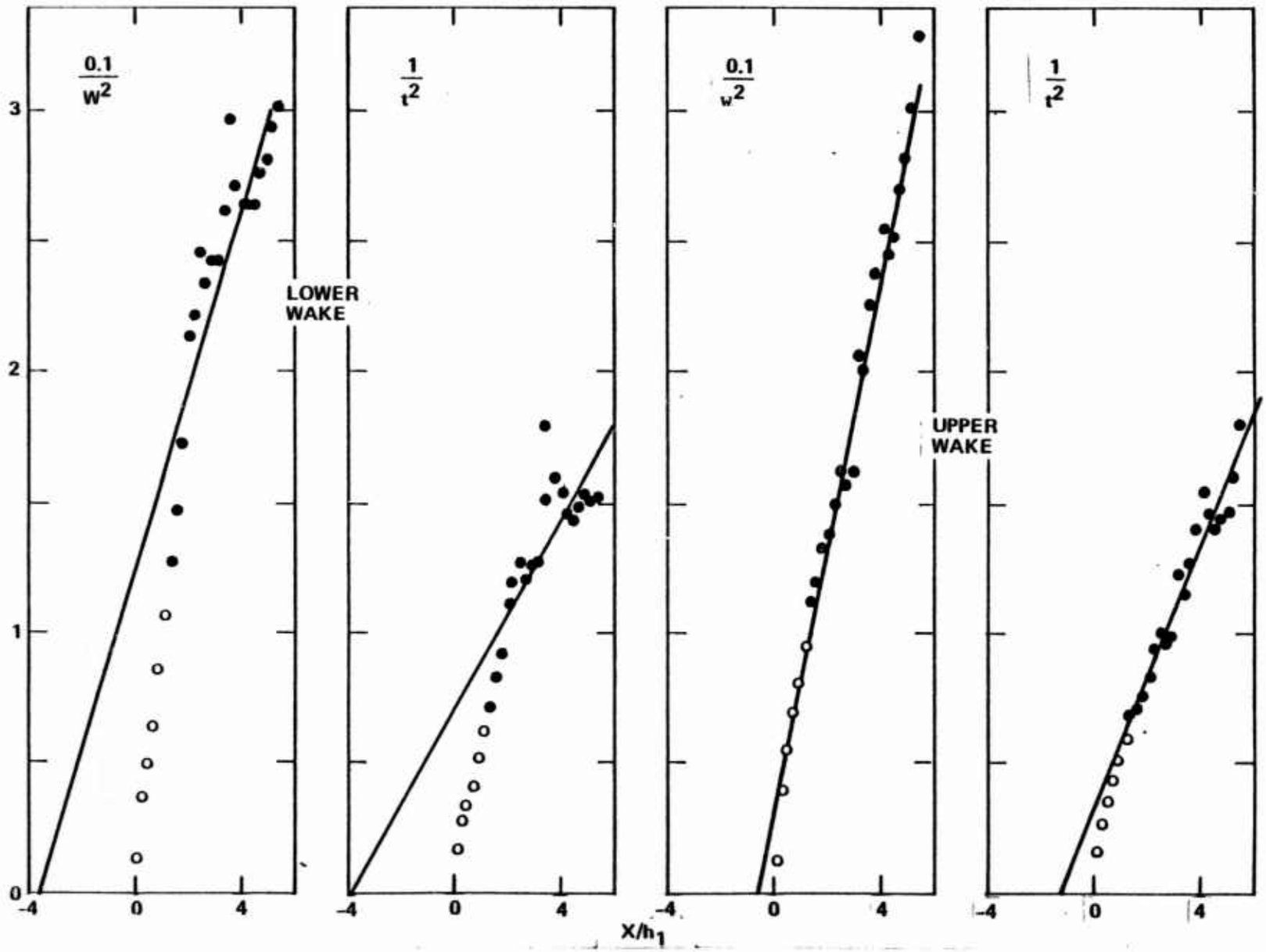

Figure 15. Search for the virtual origin of the two wakes.

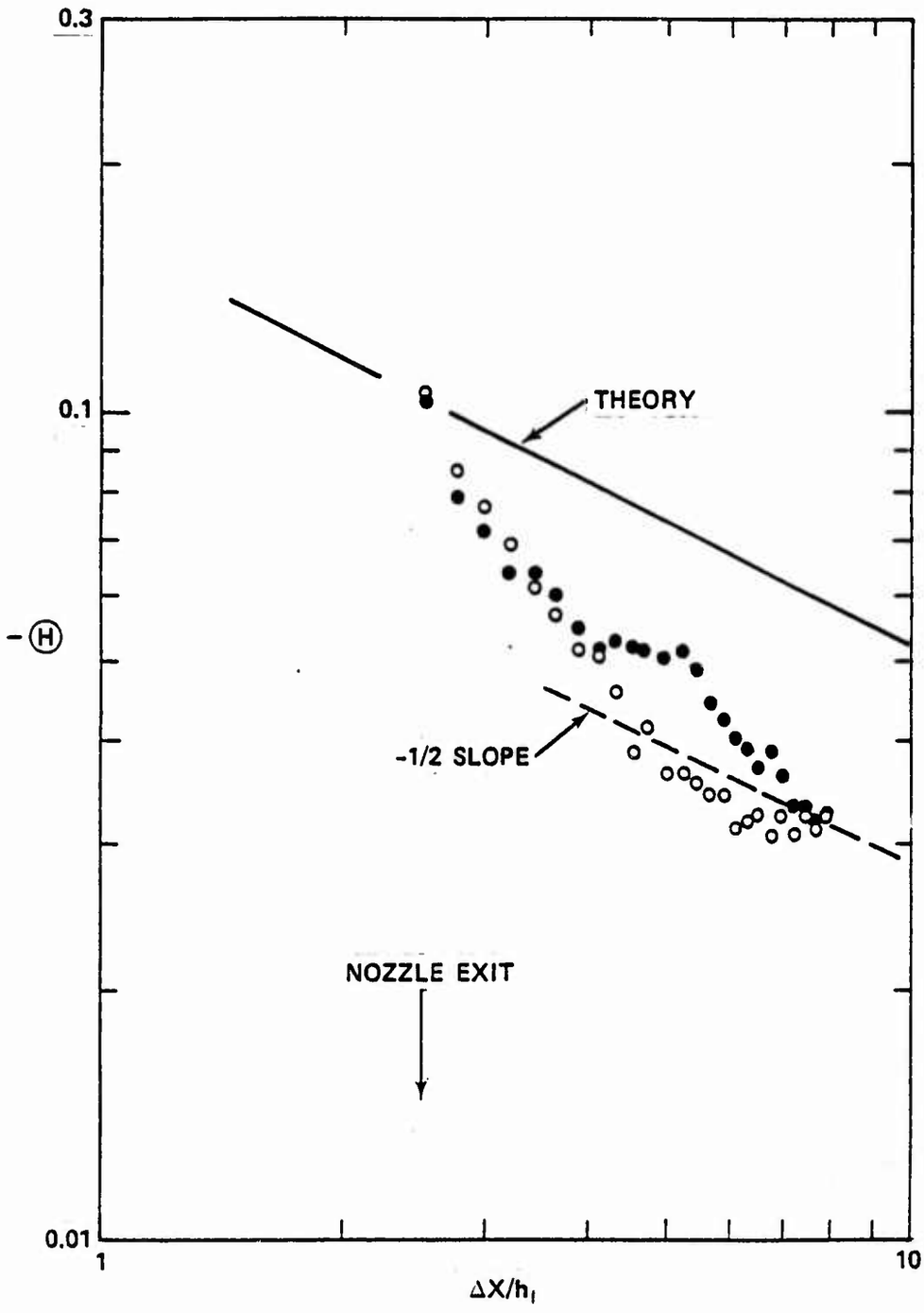

Figure 16. The total temperature defect compared with theory. Open symbols are for upper, closed symbols for lower wake.

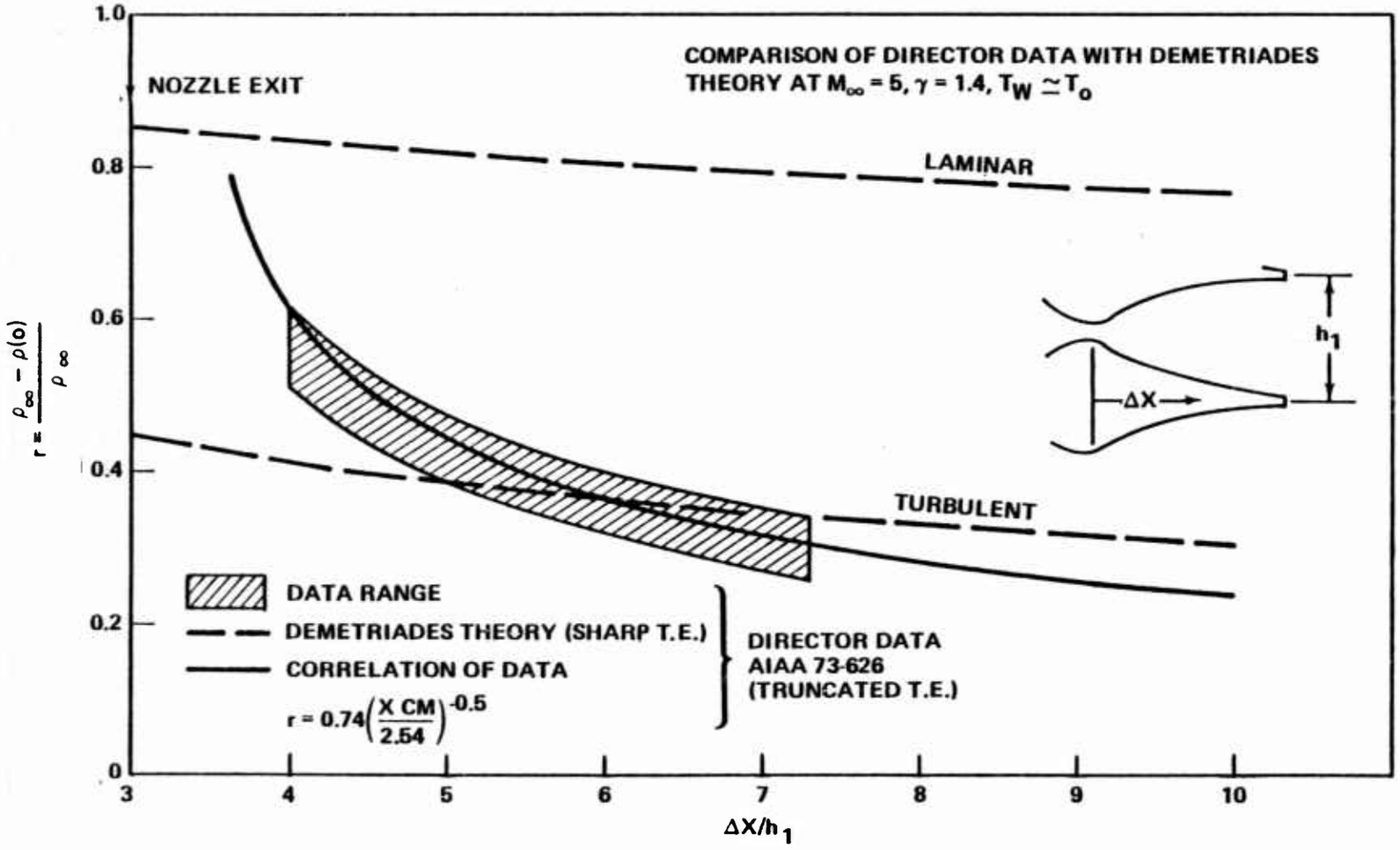

Figure 17. The data of Director compared with the Aeronutronic theory.

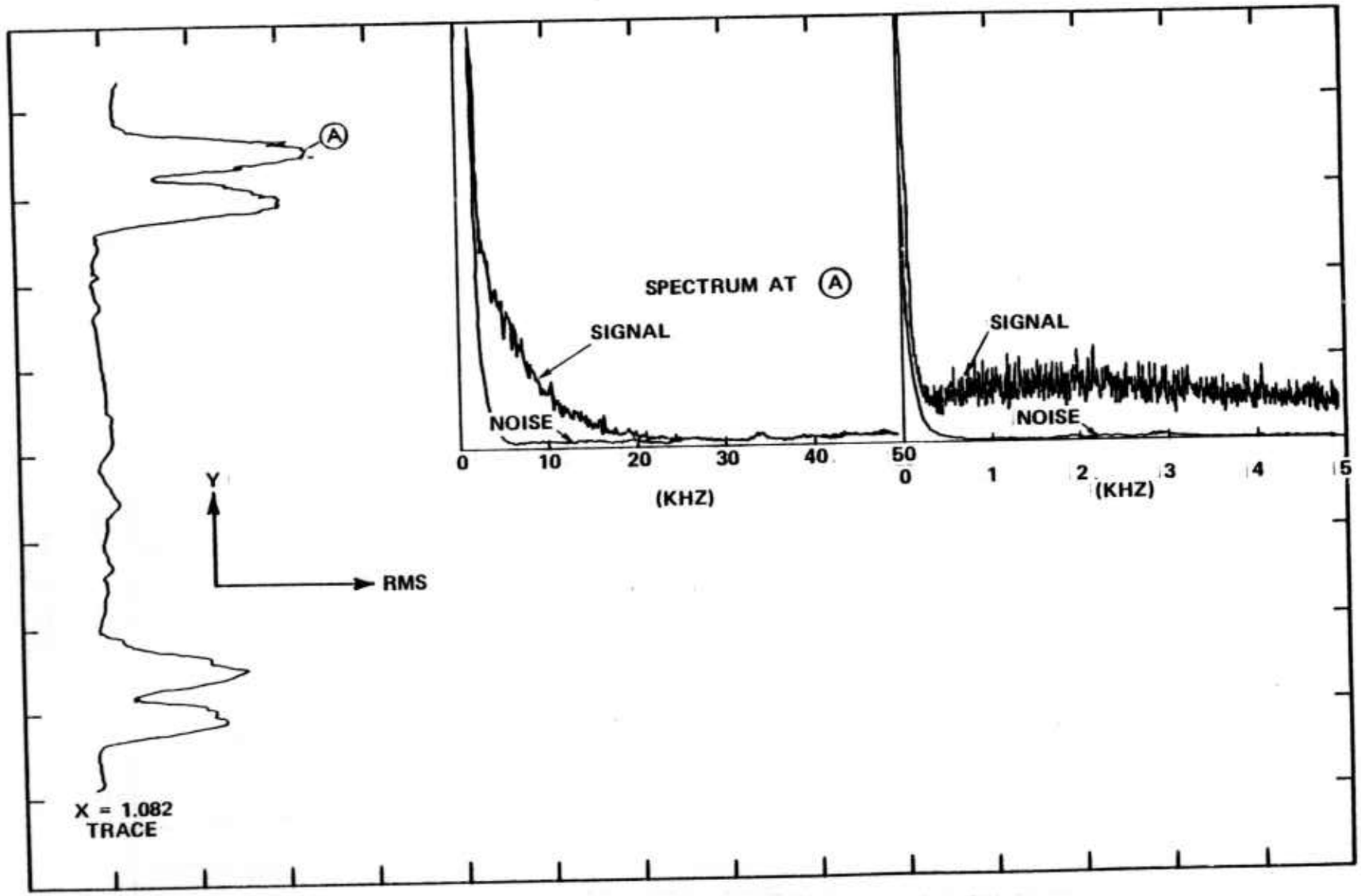

Figure 18. Hot film of the r m s fluctuations in the flow (at left) accompanied by a spectrum survey at right.

APPENDIX A

DESIGN OF THE GDL NOZZLES

A.1 DESIGN SOURCE

The nozzles were designed according to the method of two-dimensional characteristics as put forth in Shames and Seashore (reference 6). This reference designs for the shortest, highest expansion nozzles possible. Originally, the "straightforward" method of reference 6, p. 6-8, was attempted, but the wall contour resulted in a final area about 10% higher than that given for isentropic expansion. Therefore, the method finally followed is the "averaging" method.

A.2 AVERAGING METHOD

Figure A.1 shows the averaging method. The line ab is drawn from the initial wall point a, at an angle ν. Point b is the intersection of this line with the characteristic leaving the kernel at point K at an angle λ. From the midpoint c of line ab, a line is drawn at angle ν', which is the wall inclination following inclination ν in the reference 6 table. This intercepts the previous characteristic from K at B, and the new characteristic from K' (at angle λ') at d. The new wall point is B, and the new "midpoint" is e. The coordinates of the kernel points K and the initial wall point a are given in the tables of reference 6 in terms of the "half throat height" $A_t/2$, as are the angles α and λ. In the algorithm, a and B are called "wall points", b and d "far points" and c and e "midpoints".

A.3 CALCULATION ALGORITHM

A table was set up as follows:

TABLE A-I

FUNCTIONAL DIAGRAM FOR COMPUTING NOZZLE COORDINATES

ψ^-	X_k	Y_k	λ	α	$\tan\lambda_k$	$\tan\alpha$	B_k	B_w	Y	X	
								-	1	0	wall point
0	-	-	-	-	-	-	-	-	-	-	far point
								-	-	-	midpoint
								-	-	-	
0.01	-	-	-	-	-	-	-		-	-	
								-	-	-	

using the reference 6 tables (for $M_f = 4$, see p. 13-14) to list Ψ^- through tan γ (the qualities X_k and Y_k listed here are equal to $X/A_f/2$ and $Y/A_t/2$ of those tables). The last three columns were left blank. The coordinates of the first wall point, 1 and 0 were also put in. Referring to figure A.1 and Table A-I now, the equation for the lines ab and Kb are:

$$y = x \tan\alpha_a + (y_a - X_a \tan\alpha_a) = X \tan\alpha_a + B_{wa} \qquad (A.1)$$

and

$$y = x \tan\lambda_k + (y_k - X_k \tan\lambda_k) \equiv x \tan\lambda_k + B_k \qquad (A.2)$$

Since B_k, the intercept of lines passing through points K depend only on the X_k, y_k, λ_k at that point, the column B_k in Table A-I was also filled in advance:

$$B_k \equiv y_k - X_k \tan\lambda_k \qquad (A.3)$$

The steps were as follows:

(1) The intercept of line ab was determined from its definition:

$$B_w \equiv y_a - X_a \tan\alpha_a$$

$$(= 1 - 0 = 1 \text{ in this case only}) \qquad (A.4)$$

(solid lines in Table A-I)

(2) Point b was determined from the intersection on lines ab, kb, i.e., by solving simultaneously eqs. (A.1) and (A.2):

$$y_b = \frac{B_k \tan\alpha_a - B_w \tan\lambda_k}{\tan\lambda_k - \tan\alpha_a} \qquad (A.5)$$

$$X_b = \frac{B_w - B_k}{\tan\lambda_k - \tan\alpha_a} \qquad (A.6)$$

(dotted lines in Table A-I)

(3) The midpoint c was determined from:

$$X_c = \frac{X_a + X_b}{2}, \quad y_c = \frac{y_a + y_b}{2} \qquad (A.7)$$

(in this first case,

$$X_c = \frac{0 + X_b}{2} = \frac{X_b}{2}, \quad y = \frac{1 + y_b}{2} \quad)$$

(double arrows on Table A-I)

4) A new B_w is determined by using X_c, y_c and the tan α from the next line of Table A-I and apply equation (a.4):

$$B_{w_c} = y_c - x_c \tan \alpha$$

(dashed lines in Table A-I)

5) The new wall point at B is now obtained by applying formulas (A.5) and (A.6), using the values enclosed by wavy lines in Table A-I.

6) With the new wall point thus known, the procedure again begins with Step 1.

A.4 RESULTS

A.4.1 NONDIMENSIONAL COORDINATES WITHOUT VISCOUS CORRECTION

This procedure yielded the coordinates shown on Table A-II. As usual, the algorithm gave an "end" area slightly higher than that dictated for isentropic expansion to Mach 4.00; the final area ratio $A_f/A_t = 10.80$ instead of the required 10.72. This 0.7% discrepancy was corrected by displacing the last three points by a small amount, so that the final inviscid contour of Table A-II gave parallel flow at the exit. The parallel flow requirement at the nozzle exit was also imposed because we felt it a better design practice; this will be discussed further.

The inviscid length as designed is $55(A_t/2) = 27.5A_t = 2.565A_f$, which is within 2% percent of the theoretical "short nozzle" length of $2.506A_f$.

A.4.2 VISCOUS CORRECTIONS

Boundary layer displacement effects were computed assuming that the layer is laminar. A simple flat-plate approximation for δ^* was used, but utilizing the local M and unit Reynolds number R_e' at each point (reference 2):

$$\delta^* = 1.73 \frac{x}{(Re_x)^{\frac{1}{2}}} \left(1 + 1.372 \left(\frac{\gamma-1}{2}\right) M^2\right)$$

TABLE A-II

INVISCID NOZZLE COORDINATES (non-dimensional)

$\frac{x}{A_t/2}$	$\frac{y}{A_t/2}$	$\frac{x}{A_t/2}$	$\frac{y}{A_t/2}$
0	1		
.768	1.496	3.484	3.141
1.002	1.647	3.693	3.253
1.109	1.715	3.910	3.367
1.191	1.767	4.15	3.49
1.246	1.800	4.378	3.604
1.300	1.834	4.621	3.723
1.347	1.864	4.875	3.845
1.416	1.908	5.123	3.962
1.611	2.037	5.676	4.213
1.684	2.087	6.265	4.468
1.759	2.135	6.902	4.731
1.817	2.171	7.593	5.002
1.872	2.206	8.336	5.279
1.928	2.244	9.15	5.565
1.975	2.276	10.05	5.865
2.071	2.316	11.012	6.166
2.168	2.375	12.09	6.482
2.256	2.429	13.23	6.797
2.34	2.489	14.5	7.118
2.445	2.552	17.42	7.788
2.641	2.692	20.98	8.478
2.815	2.793	25.36	9.169
2.947	2.842	30.64	9.79*
3.115	2.937	37.22	10.295*
3.284	3.031	45.24	10.635*
		50.4	10.71**
		55	10.72**

*Corrected for overexpansion

**Added to ensure proper isentropic expansion

Here x, the distance from the throat, is used to compute Re_x, but $Re' = \frac{Re_x}{x}$ value comes from local conditions.

Other conditions for the calculation were $T_w = T_o = 100^oF$, $P_o = 730$ mmHg.

The resulting physical coordinates of the nozzle are shown in Table I (main text). To compute them, it was seen that the displacement thickness at the exit, $\delta_e^* = 0.0495$ inches, and the test section height $H = 3.3688$ in. Between centerlines of the cusp trailing edges, $h_1 = \frac{H}{3} = 1.1229"$.

Allowing 0.01" lip thickness, the physical half-height allowed is

$$\frac{h}{2} = \frac{1.1229-0.01}{2} = 0.5565"$$

$$h = 1.113"$$

Then, if the throat height is A_t and the flow height at the exit is h,

$$h = h_f + 2\delta^* = 10.72A_t + 2\delta^* = h$$

or

$$10.72A_t + .099 = 1.113$$

$$A_t = 0.0946"$$

Knowing A_t, the coordinates x, y of the "flow area" were computed. The physical dimensions x, $y + \delta^*$ of the nozzle were then found from δ^*. Finally, the coordinate y* from the cusp centerplane to the cusp surface (Table I) was found as an aid to the machinist.

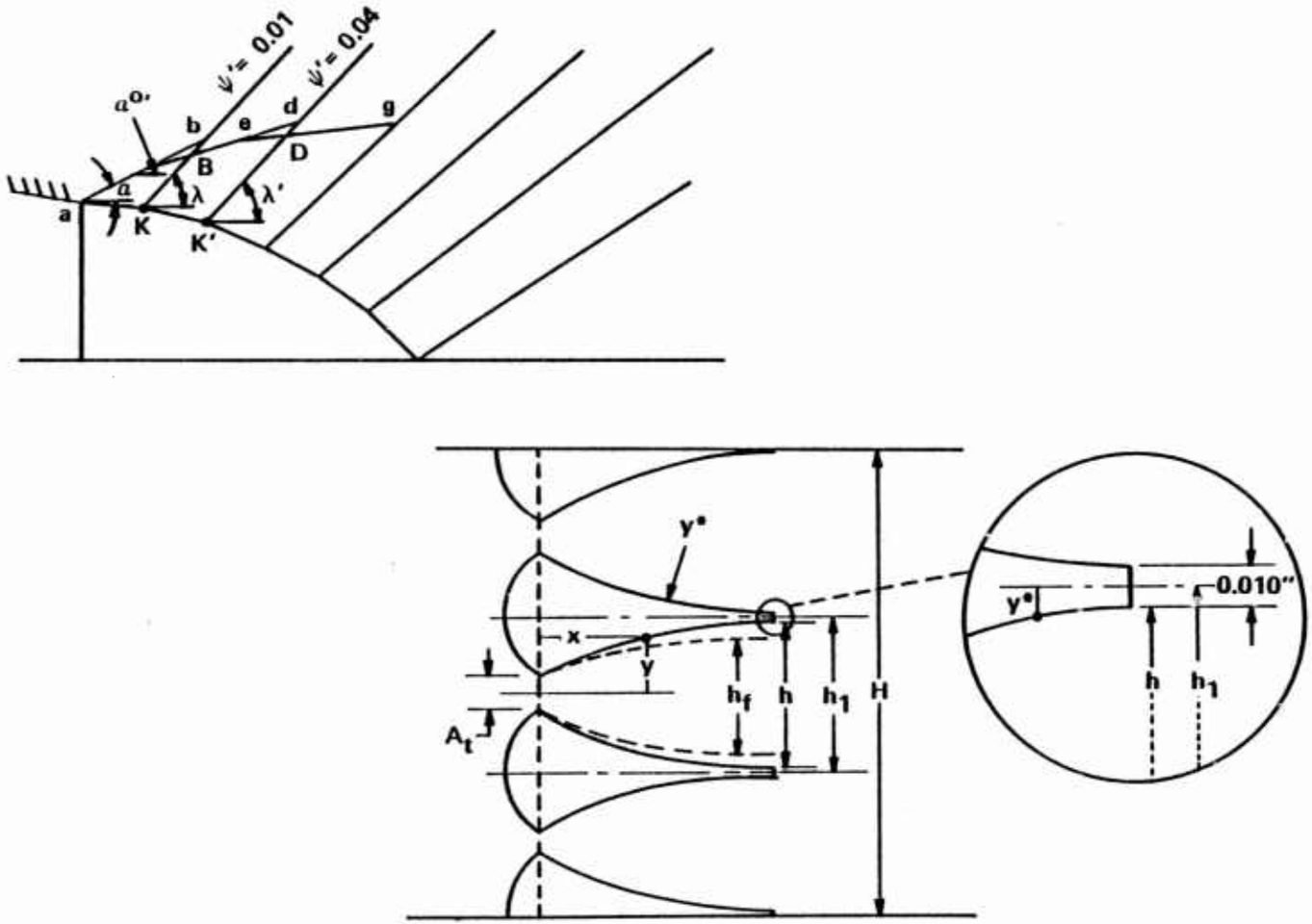

Figure A.1. Schematic of nozzle design method and coordinate nomenclature.

APPENDIX B

TRANSITION LOCATION IN THE GDL NOZZLE FLOW

B.1. PURPOSE AND METHOD

The objective was to predict the location of transition on and downstream of the GDL nozzles as presently under test. Such an estimate can be made easily if the nozzle boundary layer is approximated to a flat plate boundary layer; i.e. if each point on the nozzle is assumed to lie on a flat plate of edge M and Re' as found on that point. Standard flat plate transition correlations from experiments supplied another necessary datum, as is explained below.

B.2. TRANSITION CORRELATION

A flat plate correlation of laminar boundary layer transition, for adiabatic walls, was obtained from Coles (reference 7) in the usual form ($,_\infty$, Re_x) in the plane of Mach M and wetted Reynolds Re_x.

B.3. NOZZLE FLOW TRAJECTORY

A pair of $M_e(=M_\infty)$ and Re' (unit Reynolds number) obtains at each point on the nozzle, as well as a pair M_e and $Re_x \equiv xRe'$, where x is the distance from the throat parallel to the symmetry axis. The M_e, Re_x curve is the "nozzle trajectory" and transition is assumed to occur where this curve intercepts the transition correlation.

The procedure for plotting the M_e, Re_x curve was computerized to apply more generally. The first input was the known variation of nozzle surface contour:

$$y = y(x), \quad y^* \equiv y(x=o) = y(M=1) \tag{B.1}$$

where y* (the throat height) is another known number. The contour (B.1) was curve-fitted as follows:

$$y = \sum_n C_n x^n \qquad n=0,1,2.... \tag{B.2}$$

where C are coefficients found for each nozzle under study, and y/y* or A/A* was formed. To avoid using the implicit isentropic relation for the area ratio) where stars refer to the conditions at the throat)

$$\frac{A}{A^*} = \frac{A}{A^*}(M) \tag{B.3}$$

the relation was inverted and curve-fitted into

$$M = \sum_n B_n \left(\frac{A^*}{A}\right)^n \equiv f \text{ (isentropic area ratio)} \tag{B.4}$$

At this point, it was decided to further account for the ratio of specific heats γ, so that the final result for local M on the nozzle as a function of area ratio A/A* and γ was

$$M = \frac{f - 0.7111\gamma + 0.9956}{1.9956 - 0.7111\gamma} \qquad (B.5)$$

where f is the (inverted)isentropic M - A/A* relation from (B.4).

To proceed, the stagnation viscosity

$$\mu \equiv 1.09 \times 10^{-5} \frac{(T_o + 460)^{3/2}}{T_o + 658.6} \quad \text{cgs units} \qquad (B.6)$$

was computed, where T_o is the stagnation temperature in ^oF. Finally, the unit Reynolds number for stagnation pressure P_o at each M was found from

$$Re' \equiv \frac{P_o M}{\mu_o}\left[\frac{\gamma}{RT_o}\right]^{\frac{1}{2}} \left(\frac{T_o}{T}\right)^{-\frac{3}{2}} \frac{\frac{T}{T_o} + \frac{198.6}{T_o}}{1 + \frac{198.6}{T_o}} \qquad (B.7)$$

where the isentropic temperature ratio T/T_o is computed at M and where T_o is now in degrees Rankine.

B.4 FIRST TEST CASE: TRANSITION IN THE MACH 3.0 NOZZLE OF THE SWT

Using equation (B.7), the trajectory Re_x, M was computed for the Mach 3 nozzle. Since M = M(x), the Re_x, x trajectory was also computed and is shown on figure B.1, superposed on Cole's transition criterion. Transition is predicted when P_o = 730 mmHg absolute, but not when P_o = 200 mmHg, a verified fact.

Figure B.2 is an extension of figure B.1, plotting P_o, x instead of Re_x, x. The transition prediction is generally good at large x, judging from Schlieren data, but poorer at small x. Near the nozzle throat, especially, transition is observed to occur much earlier than predicted.

B.5 SECOND TEST CASE: MACH 4 GDL NOZZLES

Figure B.3 shows the nozzle trajectory as computed from equation (B.7) for the highest available P_o for continuous flow. The highest Re_x attained at the nozzle exit is just short of 3×10^5. The small Re_x is mainly due to the short nozzle length and, to a lesser extent, due to the decreased unit Re' for the Mach 4 operation.

Figure B.3 predicts that the GDL nozzle surface boundary layers will be laminar, assuming smooth adiabatic wall and the assumptions leading to the computation of Re'.

B.6 TRANSITION IN THE WAKES

Very slender bodies are known to produce unstable wakes at supersonic speeds, with transition Reynolds number occurring around 60,000. Since this Reynolds number is based on flow properties external to the wake and the distance from the body, transition in the GDL nozzle wakes is expected to occur within 1 cm of the cusp T.E. Generally, however, this subject is quite complex and will be approached again in a later publication.

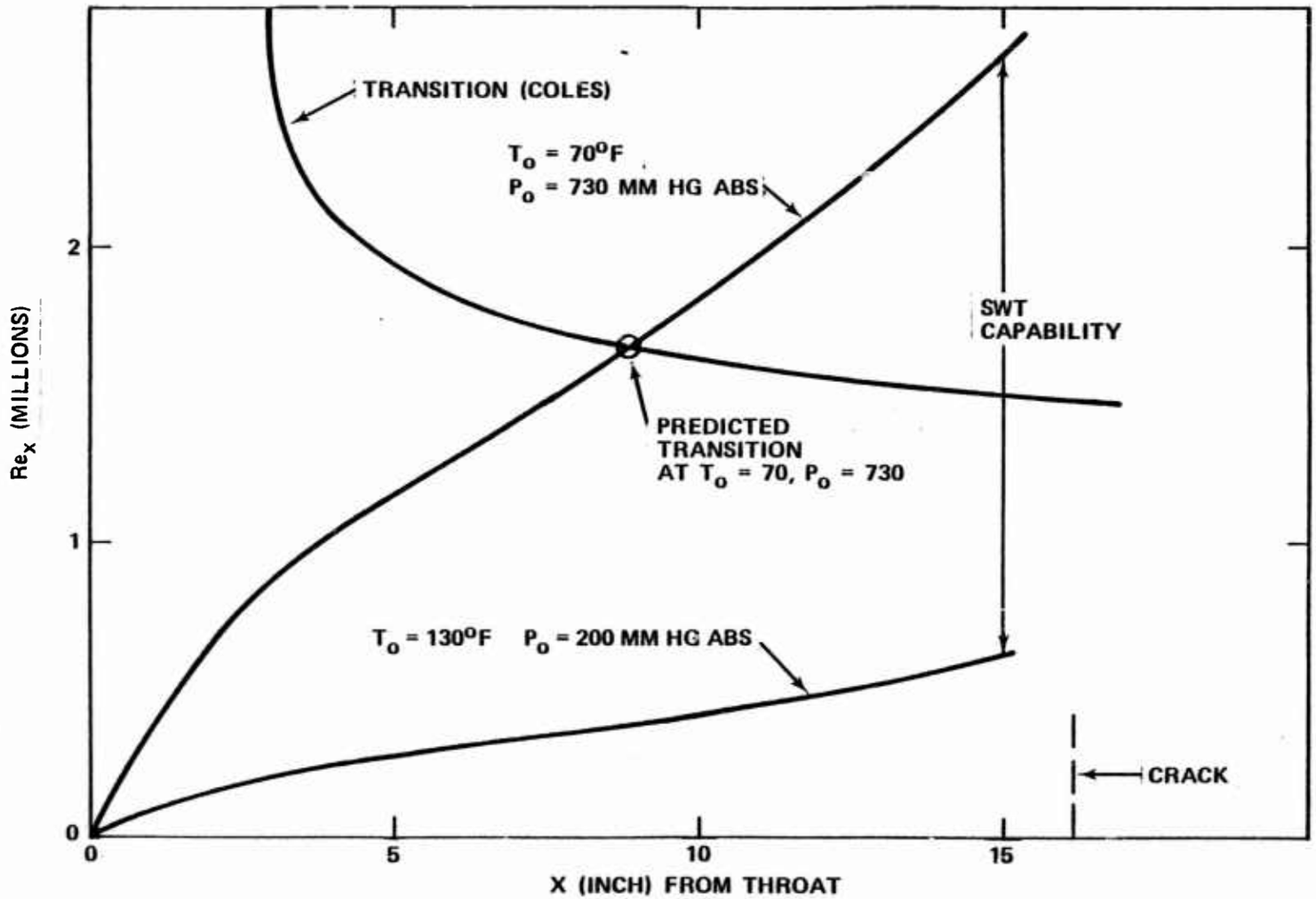

Figure B.1. Prediction of transition in the nozzle laminar boundary layer (SWT Mach 3 nozzle).

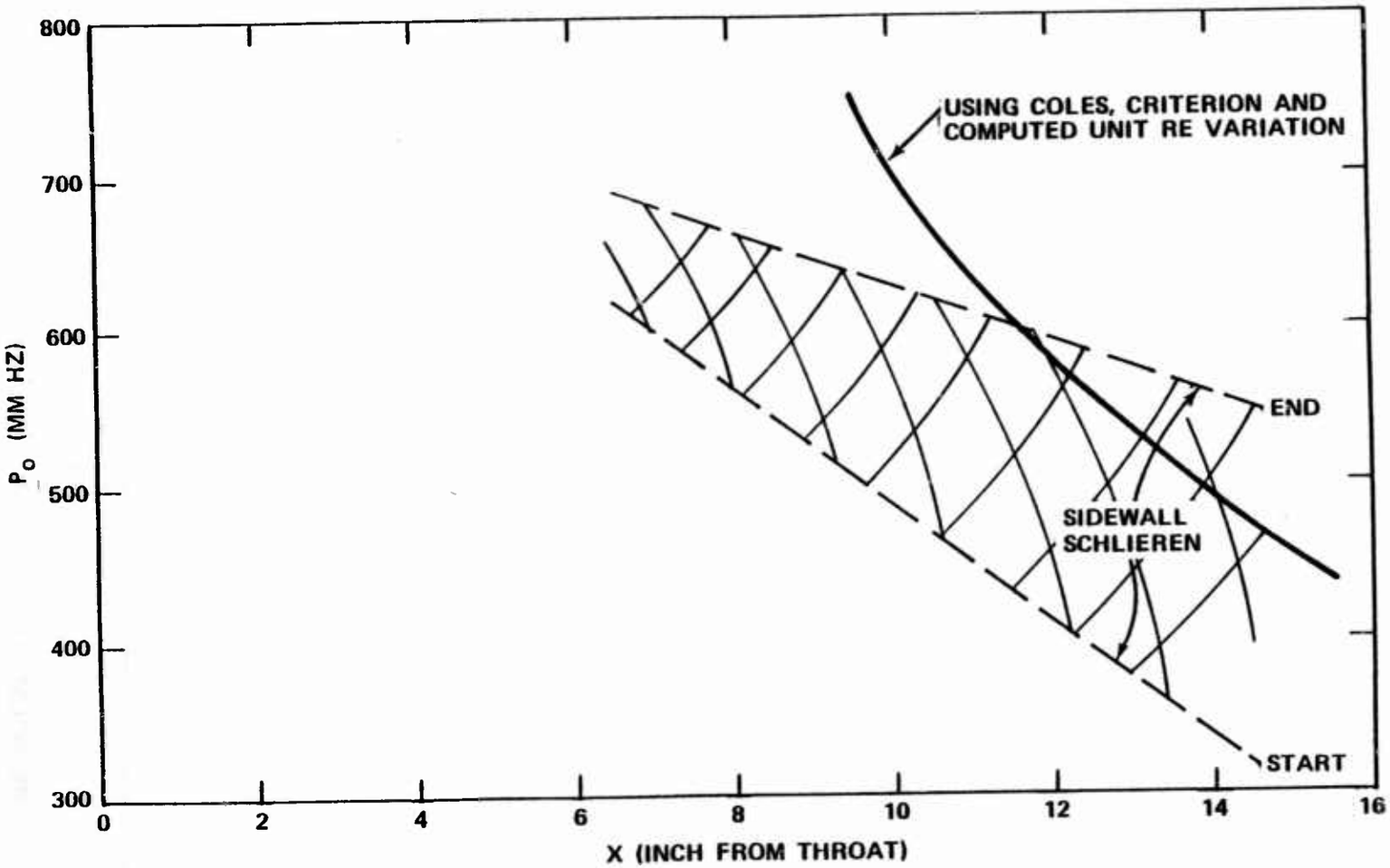

Figure B.2. Comparison of Schlieren data on the SWT Mach 3 nozzle boundary layer transition with the theoretical estimate.

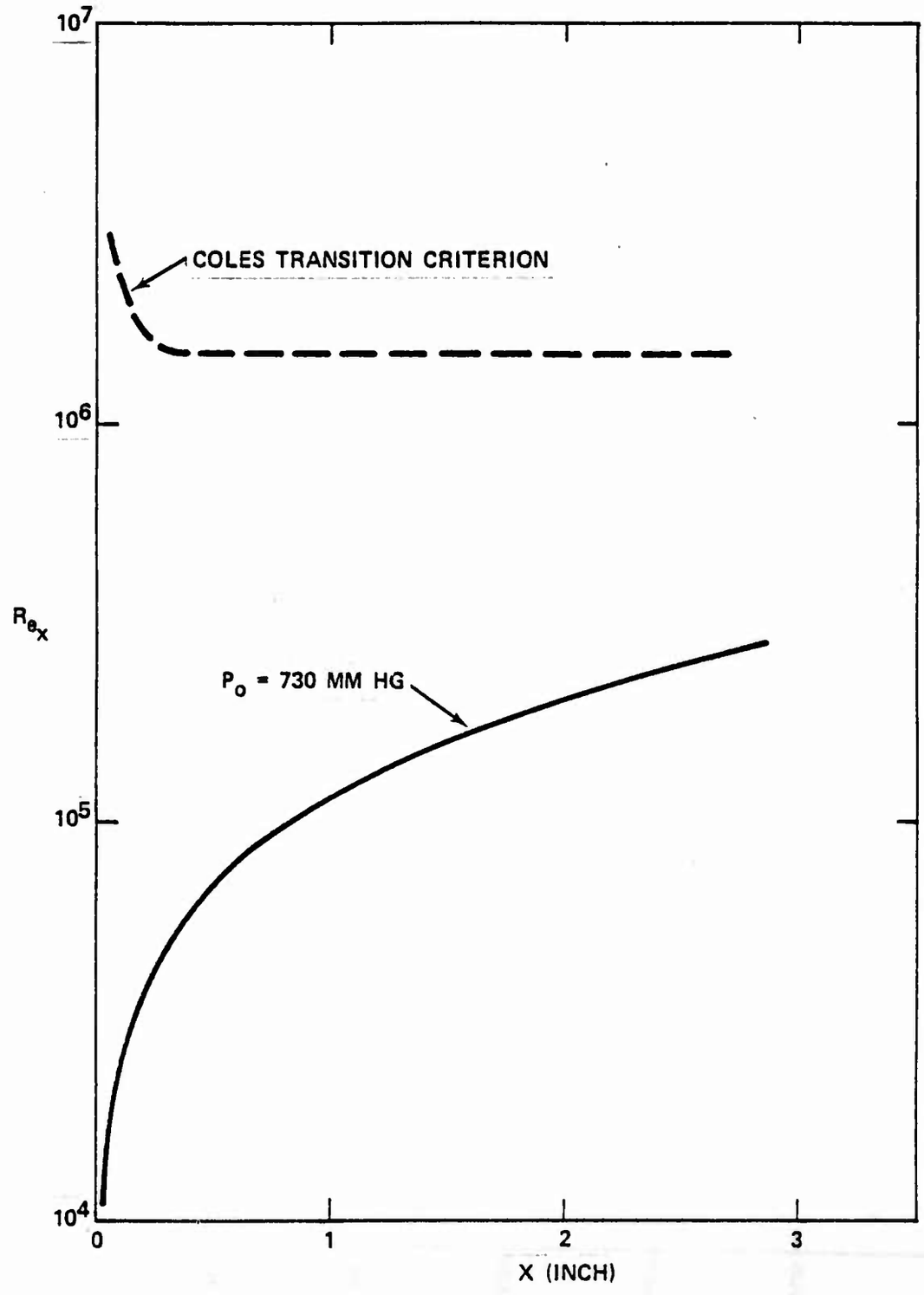

Figure B.3. Prediction of transition in the nozzle boundary layer for the Mach 4 GDL nozzles. In this case transition does not obtain.

DISTRIBUTION

DARPA, Arlington VA
ODDR&E, Wash D C
NASA (MT) Wash D C
NASA-Lewis Rsch Ctr, Cleveland OH
NASA-Langley Rsch Ctr, Hampton VA
NASA-Ames Rsch Ctr, Moffett AFB CA
R&D, Dept Army, Wash D C
DARD-ARP-P
DARD-MSA
Redstone Arsenal, AL
DRSMI-RH
AMSMI-RX
AMCPM-HEL
DRSMI-RHAL
AMCPM-HEL
NRL, Wash D C
HELPO, Wash D C
NSWC, Silver Spring MD
AiResearch, Los Angeles CA
AVCO-Everett Rsch Lab, Everett MA
Bell Aerospace Co., Buffalo NY
Boeing Co, Seattle WA
Univ Maryland, College Park MD
Ohio State Univ, Columbus OH
Calif Inst of Tech, Pasedena CA
Hughes Acft Co., Culner City CA
Inst for Def Analysis, Arlington VA
LLL, Livermore CA
Lockheed Msl & Space Co., Inc.,
Sunnyvale CA
Lockheed Rsch & Engr Ctr, Huntsville AL
NWC, China Lake CA
USAF, Wash D C
RDPS
INAKA
AFSC, Andrews AFB MD
SRLW
DLCAM
AFWL, Kirtland AFB NM
HO
SUL
ALC
SAMSO, Los Angeles CA
LASL, Los Alamos NM
Aerospace Corp., Los Angeles CA
McDonnell Douglas Rsch Lab, St Louis MO
MITRE Corp, Bedford MA
Rocketdyne, Albuquerque NM
Rocketdyne, Canoga Park CA
TRW, Redondo Beach CA
UTRC, East Hartford CT
United Tech Corp., West Palm Beach FL
Sandia Laboratories, Albuquerque NM
CALSPAN, Buffalo NY
DDC/TCA/Alexandria VA
Math Sciences NW Inc., Seattle WA
Official Record Cy, AFWL/ALC
Kirtland AFB NM